MR CAIO GUILHERME PEREIRA (Orcid ID : 0000-0003-3288-8553)

PROFESSOR HANS LAMBERS (Orcid ID : 0000-0002-4118-2272)

Article type : Research Article

Title

Trait convergence in photosynthetic nutrient-use efficiency along a 2-million year dune chronosequence in a global biodiversity hotspot

Authors

Caio Guilherme Pereira[1,2,3]*, Patrick E. Hayes[1,2,4]*, Odhran S. O'Sullivan[5,6], Lasantha K. Weerasinghe[5,7], Peta L. Clode[1,2], Owen K. Atkin[5,8] & Hans Lambers[1]

[1]School of Biological Sciences, The University of Western Australia, Crawley, Perth, WA 6009, Australia; [2]Centre for Microscopy, Characterisation and Analysis, The University of Western Australia, Crawley, Perth, WA 6009, Australia; [3]Present address: Department of Civil and Environmental Engineering, Massachusetts Institute of Technology, Cambridge, MA, 02139, USA; [4]Present address: Crop, Livestock and Environment Division, Japan International Research Center for Agricultural Sciences, 1-1 Ohwashi, Tsukuba, Ibaraki 305-8686, Japan; [5]Division of Plant Sciences, Research School of Biology, Building 134, The Australian National University, Canberra, ACT 2601, Australia; [6]Leistershire County Council, County Hall, Glenfield, Leicester LE3 8RA, UK; [7]Faculty of Agriculture, University of Peradeniya, Peradeniya, 20400 Sri Lanka; [8]ARC Centre of Excellence in Plant Energy Biology, Research School of Biology, Building 134, The Australian National University, Canberra, ACT 2601, Australia.

This is the author manuscript accepted for publication and has undergone full peer review but has not been through the copyediting, typesetting, pagination and proofreading process, which may lead to differences between this version and the Version of Record. Please cite this article as doi: 10.1111/1365-2745.13158

*Caio Guilherme Pereira and Patrick E. Hayes contributed equally to this work.

Authors for correspondence

- Hans Lambers; The University of Western Australia, Crawley, Perth, WA 6009, Australia
  Tel: +61 (0)8 6488 7381; E-mail: hans.lambers@uwa.edu.au
- Owen K. Atkin; The Australian National University, Canberra, ACT 2601, Australia
  Tel: +61 (0)2 6125 5046; E-mail: owen.atkin@anu.edu.au

Manuscript Details (Word Count)		Figures and Tables	
Main Body (excluding summary, references and legends):	6946		
Summary:	287	Number of figures:	7 (all in colour)
Introduction:	952		
Material and Methods:	1894	Number of tables:	3
Results:	1865		
Discussion and Conclusions:	2126	Number of Supplementary	7 (Fig. S1 &
Acknowledgements:	109	Information (SI) Files:	Table S1-S6)

Summary

1. The Jurien Bay dune chronosequence in south-western Australia's biodiversity hotspot comprises sites differing in nutrient availability, with phosphorus (P) availability declining strongly with increasing soil age. We have explored the exceptionally high photosynthetic P-use efficiency (PPUE) of Proteaceae in this region, triggering the question what the PPUE of co-occurring species in other families might be along the Jurien Bay chronosequence.
2. We explored how traits associated with PPUE, photosynthetic nitrogen (N)-use efficiency (PNUE) and leaf respiration might converge along the chronosequence, and whether Proteaceae and non-Proteaceae species differ in leaf traits associated with nutrient use.
3. Seven to 10 species were sampled at three sites differing in nutrient availability (ranging from N- to P-limited). Measurements of leaf light-saturated photosynthesis and dark respiration were integrated with measurements of total N and P concentration in both mature and senesced leaves, and leaf mass per unit area (LMA).
4. Contrary to what is known for other chronosequences, rates of photosynthesis and respiration did not decrease with increasing soil age and LMA along the Jurien Bay chronosequence. However, they increased when expressed per unit leaf P. Both N and P were used much more efficiently for photosynthesis on nutrient-poor sites, in both Proteaceae and non-Proteaceae species. Proteaceae had the fastest rate of photosynthesis

per unit leaf P, followed by species that preferentially allocate P to mesophyll cells, rather than epidermal cells.

5. *Synthesis.* Our results show that with declining soil P availability, PPUE of all investigated species from different families increased. Plants growing on the oldest, most nutrient-impoverished soils exhibited similar rates of CO_2-exchange as plants growing on more nutrient-rich younger soils, and extraordinarily high PPUE. This indicates convergence in leaf traits related to photosynthetic nutrient use on severely P-impoverished sites.

Keywords: Jurien Bay dune chronosequence, leaf mass per unit area, leaf respiration, nitrogen, phosphorus, photosynthesis, Proteaceae, soil development, trait convergence.

Introduction

A chronosequence is "a sequence of soils developed on similar parent materials and relief under the influence of constant or ineffectively varying climate and biotic factors, whose differences can thus be ascribed to the lapse of differing increments of time since the initiation of soil formation" (Stevens & Walker, 1970). During soil formation, the ecosystem develops, and in the long-term absence of catastrophic disturbance, a retrogressive phase follows, when plant productivity declines in response to phosphorus (P) becoming limiting (Laliberté *et al.*, 2013a, Peltzer *et al.*, 2010, Wardle *et al.*, 2004). An example is the Jurien Bay dune chronosequence in south-western Australia, uniquely located in a global biodiversity hotspot (Hopper & Gioia, 2004, Lambers, 2014, Zemunik *et al.*, 2016). Based on phytometer experiments in glasshouse studies (Laliberté *et al.*, 2012) and nutrient analyses of plants along the chronosequence (Hayes *et al.*, 2014), it was concluded that the chronosequence shows the classic pattern of a shift from nitrogen (N) limitation to P limitation of plant productivity after several thousands of years. With increasing soil age, leaf N and P concentration ([N] and [P], respectively) decline, P-resorption efficiency increases, as does the range of nutrient-acquisition strategies, with a shift towards non-mycorrhizal P-acquisition strategies (Hayes *et al.*, 2014, Lambers *et al.*, 2014, Zemunik *et al.*, 2015).

On the most severely P-impoverished sites in south-western Australia, including those along the Jurien Bay chronosequence, Proteaceae are prominent with many species showing relatively fast rates of photosynthesis per unit leaf area and a very high photosynthetic P-use efficiency (PPUE) (Denton *et al.*, 2007, Lambers *et al.*, 2012, Sulpice *et al.*, 2014). This very high PPUE is based on preferential allocation of P to mesophyll cells (Hayes *et al.*, 2018), replacement of phospholipids by other lipids during leaf development (Lambers *et al.*, 2012), and, in particular, a low investment of P in ribosomal RNA (Sulpice *et al.*, 2014) which allow a faster rate of photosynthesis per unit leaf P.

However, in these megadiverse severely P-impoverished habitats, there are many species of other families, and we know very little about their rates of photosynthesis (Veneklaas & Poot, 2003), and even less about their PPUE (Wright *et al.*, 2004). The Jurien Bay chronosequence thus offers a unique opportunity to compare the functioning of non-Proteaceae species that co-occur with Proteaceae, which we know are very efficient at using P, at sites with different levels of P availability. In particular, we can compare species with different leaf P-allocation patterns, which we know from the recent literature (Guilherme Pereira *et al.*, 2018, Hayes *et al.*, 2018). The canopy cover of non-Proteaceae decreases from almost 100% to about 65% with declining soil P availability (Lambers *et al.*, 2014). Likewise, this chronosequence provides a framework to study ecophysiological patterns in comparison with global patterns known for other chronosequences, for example, in Hawaii (Cordell *et al.*, 2001, Kitayama *et al.*, 1995, Vitousek *et al.*, 1993), Switzerland (Bernasconi *et al.*, 2011, Prietzel *et al.*, 2013), New Zealand (Atkin *et al.*, 2013, Kornfeld *et al.*, 2013, Richardson *et al.*, 2004, Richardson *et al.*, 2010, Turnbull *et al.*, 2016, Whitehead *et al.*, 2005) and Sweden (Gundale *et al.*, 2011, Lagerström *et al.*, 2013), Chile (Pérez *et al.*, 2016), and southwest China (Prietzel *et al.*, 2013, Zhou *et al.*, 2016, Zhou *et al.*, 2013).

We focused on both leaf photosynthesis and respiration of a range of species, beyond Proteaceae, across a chronosequence in a biodiversity hotspot (Lambers, 2014, Myers *et al.*, 2000). Thus we significantly expanded our work with a component not yet studied along the Jurien Bay chronosequence (Albornoz *et al.*, 2017, Hayes *et al.*, 2018, Laliberté *et al.*, 2012, 2013b, Lambers *et al.*, 2018, Li *et al.*, 2019, Png *et al.*, 2017, Teste *et al.*, 2017, Turner *et al.*, 2018, Zemunik *et al.*, 2015, 2016). We focused on traits that affect leaf carbon uptake and release, and related these to leaf [N] and [P]. We explored how those traits might converge (i.e. exhibit similar values) in different families on the most severely P-impoverished sites, and whether Proteaceae and non-Proteaceae differ in their adaptive traits associated with soil nutrient availability.

The aims of our study were to first compare species along the Jurien Bay dune chronosequence in terms of photosynthesis and respiration, to allow comparison with data on other chronosequences. We relate our findings to leaf mass per unit leaf area (LMA), leaf [N] and [P], and N- and P-resorption efficiency and proficiency. Resorption efficiency refers to the amount of nutrients remobilised during leaf senescence, relative to that in mature leaves, whereas proficiency is the final amount that remains in senesced leaves (Killingbeck, 1996, Lambers *et al.*, 2008). We hypothesise (Hypothesis 1) that non-Proteaceae species on the severely P-impoverished site show similar values for leaf traits to co-occurring P-efficient Proteaceae in terms of photosynthetic nutrient-use efficiency, nutrient concentrations in mature and senesced leaves, and LMA. Second, we aimed to explore trends in leaf traits along the chronosequence and compare these with trends

along other chronosequences. Here we hypothesise (Hypothesis 2) stronger changes with soil age along the Jurien Bay chronosequence than along other chronosequences (Atkin *et al.*, 2013, Turnbull *et al.*, 2016), first because of its stronger gradient in P availability, and, second, because there are far more species to express extreme trends than there are along other studied chronosequences. Finally, our experimental design makes it possible to explore if differences in the leaf cell-type specific allocation of P (i.e. mesophyll vs. epidermis) (Guilherme Pereira *et al.*, 2018, Hayes *et al.*, 2018) affect a plant's ability to both achieve rapid rates of photosynthesis per unit N or P and to resorb N and P. We hypothesise (Hypothesis 3) that species that exhibit preferential allocation of P to their photosynthetic mesophyll cells (Guilherme Pereira *et al.*, 2018, Hayes *et al.*, 2018) exhibit a greater PPUE and P-remobilisation proficiency. The rationale behind this is that mesophyll cells are metabolically-active cells that require most of the P in leaves, and that they are close to the phloem, used to export P; conversely, epidermal cells contain no chloroplasts and thus require little P, and are further away from the phloem.

Materials and Methods

Site description

The >2-million-year Jurien Bay dune chronosequence is located in south-western Australia, approximately 200 km north of Perth. A detailed description of the dune chronosequence is presented in Laliberté *et al.* (2012), Turner and Laliberté (2015), and Turner *et al.* (2018). Briefly, the Jurien Bay dune chronosequence comprises a series of overlapping dune systems within ~10 km of the Indian Ocean. The dunes were deposited during various periods of high sea level, from the Early Pleistocene (and possibly Late Pliocene) to the present (Wyrwoll *et al.*, 2014), and hence the age of the different dune systems increases with distance from the coast. They have been exposed to weathering since their deposition, thus creating a clear west-east soil-age gradient, which is associated with large changes in soil nutrient availability and in the type of nutrient limitation (Hayes *et al.*, 2014, Laliberté *et al.*, 2012) that match expectations from the Walker and Syers (1976) model of soil development (Turner & Condron, 2013). Plant growth is N-limited on very young dunes, co-limited by N and P on intermediate-aged dunes, and P-limited on old dunes (hundreds of thousands to millions of years old) (Hayes *et al.*, 2014, Laliberté *et al.*, 2012). The climate of the study area is Mediterranean, with hot, dry summers and cool, wet winters. Mean annual rainfall (1968–2017) is 553 mm, ~80% of which falls between May and September. Mean annual maximum temperature is 25°C, with the warmest mean monthly maximum temperature being 31°C (February) and the coolest 20°C (July).

Site and species selection

We focused on three sites, representing three of the chronosequence stages as defined in previous papers on the Jurien Bay chronosequence (Laliberté *et al.*, 2012, Turner *et al.*, 2018). Stage 1 refers to the progressive phase of very young dunes, where plant growth is limited by N; stage 3 represents the retrogressive phase of intermediate-aged dunes, where plant productivity is co-limited by N and P; while stage 4 represents old dunes, where P is the main macronutrient limiting plant productivity (Laliberté *et al.*, 2012). At each chronosequence stage, seven to 10 species were sampled that were common enough to allow sufficient replication (Table 1). At each chronosequence stage, we sought to include a range of species with contrasting leaf mass per unit leaf area (LMA) values to enable testing of relationships between leaf structure and function.

Gas exchange measurements

We quantified light-saturated net rates of leaf photosynthesis, under both ambient and saturating CO_2 concentrations (A_{sat} and A_{max}, respectively) after which dark respiration was measured (R_d). Leaf-level gas-exchange measurements were made with an infrared gas analysis system (LI-COR 6400XT, LI-COR Inc., Lincoln NE, USA), incorporating CO_2 control and a 6-cm^2 chamber, with a red-blue light source (6400-02B). All measurements were made from 11-17 November 2011, towards the end of the rainy season in this Mediterranean environment. All *in situ* gas exchange measurements were made between 10 am and 2 pm at a block temperature of 28°C. Light-saturated photosynthesis (A) was measured at 1800 µmol m^{-2} s^{-1} photosynthetic photon flux density (PPFD) at a relative humidity of 60-70%. Measurements of A were first made at an atmospheric CO_2 concentration of 400 µmol mol^{-1} CO_2 (A_{sat}); thereafter A was measured at elevated CO_2 of 1500 µmol mol^{-1} CO_2 (A_{max}); finally, leaf respiration in darkness (R_d) was measured after allowing at least 30 min of darkness before measurements commenced. A_{sat}, A_{max} and R_d were subsequently expressed on leaf area ($A_{sat,a}$, $A_{max,a}$ and $R_{d,a}$), mass ($A_{sat,m}$, $A_{max,m}$ and $R_{d,m}$), nitrogen ($PNUE_{sat}$, $PNUE_{max}$ and $R_{d,N}$) and phosphorus ($PPUE_{sat}$, $PPUE_{max}$ and $R_{d,P}$) bases. Measurements were made using undamaged, fully expanded, youngest fully-mature, and sun-exposed leaves, still attached to the plant.

Leaf mass per unit area

After completion of the gas-exchange measurements, the leaf material contained within the chamber of the LI-COR 6400XT was harvested for the analysis of structure and chemical constituents. Initially, the fresh mass was measured (Mettler-Toledo Ltd., Port Melbourne, Vic, Australia); thereafter, for situations where leaves did not fill the leaf chamber of the LI-COR 6400XT,

leaf area was determined using a LI-3100 leaf area meter (LI-COR, Inc. Lincoln, NE, USA). Subsequently, leaves were oven-dried at 70°C for 72 hours, weighed and leaf dry mass per unit area (LMA) and leaf dry matter content (DMC, ratio of leaf dry mass per unit fresh mass) were calculated. Previous studies (Dijkstra, 1998, Vile *et al.*, 2005) have shown that leaf fresh mass per unit leaf area (FMA) is a good indicator of leaf thickness, and LMA is related to FMA and DMC according to: LMA = FMA * DMC.

Leaf nutrient analyses, leaf cell-specific P allocation and nutrient-use efficiency

Leaf material from the gas exchange, LMA, FMA, and DMC measurements was used to analyse leaf nutrients. All leaf samples were oven-dried (70°C, 48 h) and finely ground in a vertical ball-mill grinder and analysed for tissue [N] and [P] using Kjeldahl acid digests (Allen *et al.*, 1974) and a LaChat QuikChem 8500 Series 2 Flow Injection Analysis System (LaChat Instruments Wisconsin, USA). Leaf [P] obtained via initial nutrient analysis were inconsistent due to analytical issues, without sufficient original leaf material left for a reanalysis. To address the absence of leaf [P] data from the 2011 samples, and also to calculate nutrient-resorption efficiency and proficiency values, mature and senesced leaves were collected from each individual plant in February 2015; these samples were collected from the same sites where the 2011 gas exchange measurements were taken. Leaf [P] is remarkably invariant from year to year along the Jurien Bay chronosequence (Table S1, Fig. S1), and very similar to values obtained before on similar sites in this severely P-impoverished region (Denton *et al.*, 2007, Sulpice *et al.*, 2014, Wright *et al.*, 2004). The temporal stability and location-specific nature of leaf [P] data justified sampling leaf P in February, 2015, and relating these values to gas exchange data from November, 2011. At each site, five healthy mature individuals were selected for most of the 2011 sampled species. As was the case in 2011, mature leaves were undamaged, fully-expanded, and sun-exposed, from the youngest, fully-matured cohort.

Senesced leaves were identified as being yellow or brown and detached easily from the plant. Where possible, senesced leaves were collected directly from the plant by gently shaking the plant and collection of fallen leaves; alternatively, where this was not possible, senesced leaves were collected directly from recently-fallen litter beneath the plant. Senesced leaves collected from this litter showed no visible degradation, and because they had likely fallen over summer, they had not been exposed to any significant rain between litter fall and collection. We therefore assume a minimal loss of nutrients through leaching or decomposition, although some photodegradation may have occurred (Austin & Vivanco, 2006, Gliksman *et al.*, 2016). A total of 180 leaf samples (mature and senesced) were collected for nutrient analysis in 2015; both sets of leaves were oven-dried

(70˚C, 48 h) and finely ground in a vertical ball-mill grinder using plastic vials and yttria-stabilised zirconia ceramic beads. A subsample was acid digested using concentrated HNO_3:$HClO_4$ (3:1) and the leaf [P] determined colourimetrically using malachite green method (Motomizu *et al.*, 1983). A second subsample was analysed for leaf [N] using a LaChat QuikChem 8500 Series 2 Flow Injection Analysis System (Lachat Instruments Wisconsin, USA) using Kjeldahl acid-digestion (Allen *et al.*, 1974).

To calculate rates of leaf gas exchange per unit leaf P, individual gas exchange rates were divided by site-species mean values of leaf [P] obtained in 2015. For rates of gas exchange per unit leaf N, we used individual leaf N values from the 2011 collected plants. For resorption, we used N data from the 2015 sampled leaves.

In terms of leaf cell-specific nutrient-allocation patterns, species were grouped according to their relative allocation of leaf P to mesophyll versus epidermal cells, i.e. species in which the cellular [P] of the epidermis was either higher or equivalent to that of the mesophyll (M ≤ E) and species in which the cellular [P] was significantly higher in the mesophyll (M > E). The leaf nutrient-allocation patterns of *Acacia rostellifera, Anthocercis littorea, Myoporum insulare, Olearia axillaris, Spyridium globulosum, Templetonia retusa, Melaleuca systena* and *Labichea cassioides* are described in Guilherme Pereira *et al.* (2018), whilst those of *Banksia prionotes* and *Hakea incrassata* are in Hayes *et al.* (2018). Plants from the same genus collected in the present study (namely *Acacia lasiocarpa, Banksia nivea* and *Banksia leptophylla* var. *melletica*) were considered as having the same leaf P-allocation pattern of the congeneric species. The Proteaceae species (*Conospermum stoechadis*) was also considered to preferentially allocate its P to mesophyll cells (Hawkins *et al.*, 2008, Hayes *et al.*, 2018, Lambers *et al.*, 2015, Shane *et al.*, 2004).

In this study, non-Proteaceae species were considered 'efficient' in the use of P whenever the species mean PPUE ≥ 200 μmol CO_2 g^{-1} P s^{-1}. This value was approximately the median for all analysed species in the study, as well as two-fold greater than the mean of all plant species described in the Glopnet dataset (Wright et al. 2004).

Leaf section preparation and imaging

Small (≈5 × 5 mm) leaf sections of three species with highly different morphologies (*Banksia prionotes*, *Acacia rostellifera* and *Melaleuca systena*) were also collected at the stage 4 site for anatomical imaging. The samples were immersed in fixative (2.5% glutaraldehyde/1.6% paraformaldehyde in 10 mM phosphate buffer) and left at room temperature for 24 h before being stored at 4°C until further processing. Fixed leaves were then cut using a vibratome to produce transverse leaf sections of ≈30 -60 μm. These were mounted in water on glass slides and imaged

using brightfield and fluorescence (ultraviolet excitation) illumination on an Axioskop optical microscope (Zeiss, Oberkochen, Germany) fitted with an Axiocam digital camera (Zeiss), or prepared for scanning electron microscopy, by being dehydrated through a graded series of ethanols, critical point dried, coated with Au, and imaged at 5 kV in a field emission SEM (Zeiss).

Statistical analyses

Leaf-trait (LMA, FMA, DMC, leaf [N], leaf [P], and N:P ratio), physiological parameters (A_{sat}, A_{max} and R_d expressed on leaf area, mass, N and P bases) and nutrient-resorption data (N and P resorption efficiency/proficiency) were analysed using linear mixed-effect models (GLMM; McCulloch and Neuhaus, 2005). Different models were fitted to the data, taking into account the parameter to be analysed and the stages of soil development, with species as the random effect. This method was also applied to determine differences between species with contrasting cell-specific P-allocation patterns and among distinct plant groups (non-efficient non-Proteaceae, efficient non-Proteaceae, and Proteaceae) in terms of mature and senesced total leaf P, P-resorption efficiency, and PPUE. The significant models were selected using Akaike's Information Criterion (AIC; see Supplementary Tables S2-S6 for the models' details). Models were screened for normality and homoscedasticity of the residuals (Zuur et al. 2009), and appropriate variance structures were applied whenever necessary. Differences among distinct soil-development stages (Figs 1, 3-4), species with contrasting leaf cell-specific P-allocation patterns (Fig. 6), and plant groups with P-use efficiency (Fig. 7) were determined through Tukey's HSD post-hoc tests, after it had been determined that all assumptions of this test were met. Correlations between photosynthetic nutrient-use efficiency (for N and P) and nutrient-resorption proficiency (Fig. 5) were performed using mean values for each species and thus intrinsically estimated with errors, which led us to opt for model II regression (with the parameters being estimated with ordinary least squares (, Powell *et al.*, 2015)). The influence of possible outliers was analysed through Cook's distances (D_i), and although *Acacia lasiocarpa* and *Olearia axillaris* had relatively high D_i values (0.34 and 0.26, respectively), including them had no effect on the model's significance. The linear mixed-effect models were created with the lme4 package ( ), whilst the model II regressions were performed with the lmodel2 package. All statistical analyses were performed in the *R* Environment (R Development Core Team 2017).

Results

Leaf structural and chemical composition traits

Table 1 shows species mean values of leaf structural and chemical composition traits at each of the three chronosequence stages (stage 1, very young dunes; stage 3, intermediate-aged dunes; and, stage 4, old dunes). For each trait, Tables S2-S6 show results of the mixed-effects models used to test whether there were significant differences among the three stages.

Within each chronosequence stage, species-mean values of LMA varied two- to three-fold among co-occurring species, ranging from 87 g m^{-2} (*Dioscorea hastifolia*) at stage 1, to 308 g m^{-2} (*Hakea incrassata*) at stage 4 (Table 1). When averaged across all species within each stage, LMA values were lowest for plants at the two youngest sites and significantly higher at the oldest site (Fig. 1a). Fresh mass per unit leaf area (FMA), a proxy for leaf thickness, was similar at all sites (Fig. 1b), and therefore variation in LMA was accounted for by variation in DMC, which showed a pattern very similar to that of LMA (Fig. 1c).

Across the chronosequence, dry mass-based leaf [N] and [P] varied from *ca*. 6 to 20 mg N g^{-1} and 0.3 to 2.1 mg P g^{-1}, respectively (Table 1). Values for mature leaf [N] and [P], averaged for all species measured at a specific site, declined with increasing soil age, when expressed on a mass basis (Figs 1d,e) as well as on an area basis (data not shown); the leaf N:P ratio was lowest on the youngest stage, higher on the intermediate stage, and highest on the oldest stage (Fig. 1f). These results are consistent with previous results (Fig. S1), where different species were measured at different sites along the same chronosequence (Hayes *et al.*, 2014).

Since very few species occur on all studied sites, a detailed comparison of single-species performance across the sites was not possible. Only *Acacia rostellifera* occurred on all sites investigated, exhibiting LMA values varying from 136 g DM m^{-2} at the youngest site (stage 1), 126 g DM m^{-2} at the site with intermediate age (stage 3) to 155 g DM m^{-2} at the oldest, stage 4 site (Table 1). Values for LMA of *Anthocercis littorea* were lower at the oldest site than at the youngest site (stage 1), but those of *Banksia nivea* were higher at the oldest compared with the intermediate site (Table 1). Leaf DMC of the same three species showed similar values among sites. *Melaleuca systena* showed a lower LMA value at the intermediate site (178 g DM m^{-2}) than at the oldest site (295 g DM m^{-2}); this was mainly accounted for by a higher DMC (Table 1). For *A. rostellifera,* mass-based leaf [N] values were similar across the three sites, with leaf [P] values declining by ~33% with increasing soil age (Table 1). *Melaleuca systena* showed a decrease in leaf [N] from 12 mg g^{-1} to 9.3 mg g^{-1} with increasing soil age. Therefore, the trend of increasing LMA and DMC, decreasing leaf [N] and [P], and increasing N:P ratio as shown in Fig. 1, predominantly reflects a change in species with increasing soil age (inter-species differences), rather than changes within single species (intra-species differences).

To gain further insight into the structure of species adapted to low-nutrient conditions along the chronosequence, the gross cellular morphology of leaves from three species at the site where mean N:P ratios were greatest was investigated. *Banksia prionotes* showed a dorsiventral leaf anatomy, with lignified and thick-walled fibrous bundles dividing mesophyll tissue; this was the only species to show sunken stomata in stomatal crypts on the abaxial surface (Figs 2a-c,f,i). *Acacia rostellifera* showed flat isobilateral leaves, with two layers of mesophyll cells at the surface, and parenchyma tissue inside (Figs 2d,e). *Melaleuca systena* showed isobilateral ellipsoid leaves, with a double layer of mesophyll cells at the outside, and parenchyma cells inside (Figs 2g,h).

Leaf gas exchange

Table 2 shows site-mean values of leaf gas exchange for each of the sampled species. Across all species and sites, area-based rates of light-saturated photosynthesis, measured under ambient [CO_2] ($A_{sat,a}$), ranged from 6.5 to 26.7 μmol m^{-2} s^{-1}. Within the intermediate and the oldest site, a 1.3- to 1.65-fold variation in rates of A_{sat} was observed among co-occurring species. Interestingly, the site-mean $A_{sat,a}$ values were similar across sites (Fig. 3a; Table S3), despite the major increase in LMA and decrease in leaf [N] and [P] with increasing soil age (Fig. 1). Site-averaged mass-based rates of A_{sat} ($A_{sat,m}$) were also similar at all chronosequence stages (Fig. 3b), suggesting that the significant differences in LMA among sites (Fig. 1a) were insufficient to result in significant differences in mass-based photosynthesis measured at ambient atmospheric [CO_2]. Rates of photosynthesis per unit N (Fig. 3c) and P (Fig. 3d) were significantly slower at the youngest site than at the other two older sites.

As noted above, a comparison of single-species performance across the sites was not possible, except for *Acacia rostellifera*, which showed $A_{sat,a}$ rates varying from 17.8 μmol m^{-2} s^{-1} at the youngest site to 23.9 μmol m^{-2} s^{-1} at the oldest. Likewise, *A. littorea* showed a 9% faster $A_{sat,a}$ at the oldest site, and *Banksia nivea* exhibited a $A_{sat,a}$ value that was 48% higher at the oldest compared with the intermediate site (Table 2). Therefore, the maintenance of site-mean area-based rates of photosynthesis across the chronosequence (for the selected species used in our study) was not necessarily due to individual species exhibiting identical rates among sites. Rather, the maintenance of site-mean $A_{sat,a}$ likely reflects differences in species composition among sites, with differences in leaf anatomy playing a role. Interspecific differences in leaf anatomy (Fig. 2) could contribute to the maintenance of site-mean $A_{sat,a}$ (Fig. 3a) across the chronosequence. For example, the stomatal crypts of *Banksia prionotes* likely aid CO_2 diffusion into leaves of a species that otherwise has a 'non-efficient' cellular distribution (Hassiotou *et al.*, 2009). Similarly, isobilateral anatomy of *Acacia rostellifera* and *Melaleuca systena*, in which both palisade mesophyll layers are

very close to the leaf surface, likely minimises barriers to CO_2 diffusion. Species with needle-like leaves, in which the mesophyll is positioned at the most outer area of the leaf, also likely maximise gas diffusion.

The highest values of area-based photosynthesis of all species and sites were exhibited by *Acacia lasiocarpa* (Fabaceae) (26.7 μmol m^{-2} s^{-1}), which was measured only at the site of intermediate age (Table 2). The next-highest $A_{sat,a}$ values were shown by *Acacia rostellifera* and *Melaleuca systena* (Myrtaceae) (both 23.9 μmol m^{-2} s^{-1}) at the oldest site; however, since mass-based rates of photosynthesis for *Melaleuca systena* were not among the highest, it is likely that the leaf area of these plants, which have small ellipsoid leaves (Fig. 2), was underestimated, and hence this species was excluded from Fig. 3 when values are shown on an area basis, but included when showing values expressed on a different basis (e.g., mass, N or P). *Clematis linearifolia* (Ranunculaceae) also exhibited rapid rates (23.2 μmol m^{-2} s^{-1}), measured at the intermediate-age site, and *Banksia prionotes* (23.1 μmol m^{-2} s^{-1}) and *Banksia nivea* (23.0 μmol m^{-2} s^{-1}) showed equally high $A_{sat,a}$ values, both measured at the oldest site (Table 2). The two *Banksia* species (Proteaceae) at the oldest site are remarkable in that they achieved these fast rates with much lower leaf [N] and [P] than the other species exhibiting rapid rates of photosynthesis (Tables 1 and 2).

Leaf respiration measured in the dark showed a similar pattern as photosynthesis (Fig. 3e-h), with subtle differences, referred to below. A near eight-fold range was seen in species average values of area-based rates of respiration ($R_{d,a}$, Table 2). The lowest values of $R_{d,a}$ of all species and sites were exhibited by *Phyllanthus calycinus* at the site of intermediate age (1.1 μmol m^{-2} s^{-1}), followed by *Spyridium globulosum* at the site of intermediate age and *Dioscorea hastifolia* (both 1.2 μmol m^{-2} s^{-1}), which was measured only at the youngest site (Table 2). The next lowest value was shown by *Banksia prionotes* at the oldest site (1.3 μmol m^{-2} s^{-1}). Very high values were shown by *Acacia lasiocarpa* (8.4 μmol m^{-2} s^{-1}) and *Melaleuca systena* (6.1 μmol m^{-2} s^{-1}), both at the site of intermediate age, and *Melaleuca systena* (5.0 μmol m^{-2} s^{-1}) at the oldest site (Table 2); values for *Melaleuca systena* were not included in Fig. 3a,e, for the reason explained above. When assessed using site-mean values, no significant differences were found among the chronosequence stages, either in area or mass-based rates of leaf R_d (Fig. 3e,f).

Leaf respiration, measured in darkness, expressed as a fraction of light-saturated photosynthesis (A_{sat}) varied markedly among the selected species, with R_d/A_{sat} ratios ranging from as low as 0.06 (*Banksia prionotes*) to as high as 0.55 (*Banksia leptophylla*) (Table 2). At the site-mean level, R_d/A_{sat} ratios also varied with soil age, being significantly less in stage 3 than in stages 1 and 4; the mean values were 0.14, 0.11 and 0.15 for Stages 1, 3 and 4, respectively.

Nutrient-resorption efficiency and proficiency

Senesced leaf [N] and [P] declined sharply with increasing soil age, and the resorption efficiency increased, especially for P (Fig. 4). To test if there was a trade-off between photosynthetic N- and P-use efficiency (PNUE and PPUE, respectively) and N and P remobilisation, we plotted PNUE vs N-resorption proficiency, i.e. the final amount of N left in senesced leaves (Fig. 5a), and PPUE vs P-resorption proficiency (Fig. 5b), i.e. the final amount of P left in senesced leaves. Figure 5a shows that variation in PNUE and senesced leaf N were unrelated, suggesting no evidence of a trade-off. By contrast, PPUE decreased with increasing senesced leaf P; thus, PPUE was highest in species that showed the highest P-remobilisation proficiency (i.e. they both used and remobilised P effectively).

Figure 6 shows leaf [P] in mature and senesced leaves, grouped according to the relative cell-specific allocation of P to mesophyll versus epidermal cells. In both mature and senesced leaves, [P] were significantly higher in species that allocate relatively more P to epidermal than mesophyll cells (Fig. 6a,b). Associated with the higher [P] in epidermal cells were significantly lower P-resorption efficiency (Fig. 6c) and significantly lower PPUE (Fig. 6d). Thus, interspecific differences in how P is allocated among different cell types may be a major factor influencing the efficiency of P use in mature leaves, as well as the fraction of P resorbed from leaves as they senesce.

To compare how non-Proteaceae and Proteaceae differed in patterns of P use and resorption, we analysed mature leaf [P] (Fig. 7a), senesced leaf [P] (Fig. 7b), P-resorption efficiency (Fig. 7c), and PPUE (Fig. 7d) for non-Proteaceae species grouped into those with mean PPUE values below and above 200 µmol CO_2 g^{-1} P s^{-1} (non-efficient and efficient, respectively). These were compared with values for Proteaceae species. As expected, Proteaceae species exhibited low [P] in mature and senesced leaves, and high PPUE. Interestingly, the 'efficient' non-Proteaceae species also exhibited low mature and senesced leaf [P]. However, no differences were found among the three groups with respect to P-resorption efficiency (Fig. 7c). This may be because the [P] in both mature and senesced leaves were greater in inefficient non-Proteaceae, giving the same P-resorption efficiency, but greater P-resorption proficiency in efficient species.

Discussion

Leaf nutrient concentrations decreased and LMA increased with increasing soil age, as found in other chronosequence studies, but the decrease in leaf nutrient concentrations was much stronger than found along chronosequences in Chile and New Zealand, supporting Hypothesis 2 that there would be stronger changes with soil age along the Jurien Bay chronosequence than along other chronosequences (Eger *et al.*, 2013, Pérez *et al.*, 2016, Richardson *et al.*, 2004, Whitehead *et al.*, 2005). Key findings of our study are that rates of photosynthesis and respiration expressed per unit

leaf area or mass did not decrease with increasing soil age and LMA along the Jurien Bay soil chronosequence. This differed from what is known for other chronosequences (Atkin *et al.*, 2013, Pérez *et al.*, 2016, Turnbull *et al.*, 2016, Whitehead *et al.*, 2005). The performance of the species in terms of rapid area-based rates of photosynthesis, low [N] and [P], and a high LMA on the oldest dunes also differed from that of other plant species with low leaf nutrient concentrations (Wright *et al.*, 2004) or a high LMA (Evans, 1989). Most importantly, both N and P were used much more efficiently for photosynthesis on sites with lower nutrient availability in both non-Proteaceae and Proteaceae species (supporting Hypothesis 1), with the Proteaceae having the greatest PPUE, because they functioned at lower leaf [P] than non-Proteaceae species.

Plant traits related to productivity: LMA and photosynthesis

In our study, plant productivity is expected to be greatest at the youngest site (Stage 1), the progressive phase of ecosystem development, where foliar [P] are at their maximum (Hayes *et al.*, 2014, Richardson *et al.*, 2004, Wardle *et al.*, 2004). Such greater plant productivity cannot be accounted for by faster area-based rates of photosynthesis; instead it would be explained by low values of LMA and associated rapid rates of mass-based photosynthesis, which are typical for fast-growing species (Lambers & Poorter, 1992). The low LMA was due to a low DMC (Fig. 1), indicating less investment in non-productive cell types such as those found in sclerenchymatic tissues (Witkowski & Lamont, 1991), as is typical for faster-growing species (Lambers & Poorter, 1992). Based on measured rates of photosynthesis and LMA values, plant productivity is expected to also be relatively high at the site of intermediate age, where N and P are co-limiting (Hayes *et al.*, 2014, Laliberté *et al.*, 2012). The lowest productivity is expected at the oldest site, the retrogressive phase of ecosystem development where LMA values were highest and foliar [N] and [P] lowest (Fig. 1). Yet, photosynthesis rates (expressed on area, mass, N and P bases) were not significantly slower at this site (Fig. 3). In our study, we measured photosynthesis at a favourable time of the year when there was still enough soil moisture available. The differences in photosynthesis rates among chronosequence stages and species may well be somewhat different later during the year in this Mediterranean environment with little summer rain, as reported by Veneklaas and Poot (2003) for a nearby site. However, our aim was to compare photosynthetic nutrient-use efficiency of Proteaceae and non-Proteaceae under defined conditions, rather than seasonal variation in gas exchange.

To survive under conditions of low nutrient supply, drought, and high temperatures common in the Jurien Bay area, leaves would be expected to exhibit high LMA values relative to species occurring in more favourable environments (Hypothesis 1). Yet, LMA values of some of the

selected species were not particularly high (Table 1). For example, *Anthocercis littorea* exhibited relatively low LMA values, both at the youngest and oldest sites. *Anthocercis littorea* is a fire ephemeral (Pate *et al.*, 1985), restricted to disturbed sites along the chronosequence. Its leaves contain atropine and a range of other alkaloids (Aplin & Cannon, 1971, Evans & Ramsey, 1983, Evans & Treagust, 1973, Evans & Woolley, 1969); these alkaloids likely confer protection against herbivory, reducing the need for a high LMA (Bermúdez-Torres *et al.*, 2009). Similarly, *Templetonia retusa* also shows a strongly positive test for alkaloids, while *Myoporum* species give moderately or weakly positive tests (Aplin & Cannon, 1971). Yet, alkaloid concentrations do not explain the observed low LMA values of all species along the chronosequence, with *Dioscorea hastifolia*, *Phyllanthus calycinus* and *Spyridium globulosum* exhibiting relatively low LMA without producing alkaloids (Aplin & Cannon, 1971). Here, factors other than alkaloids likely contribute to the ability of these species to tolerate the harsh conditions found along the Jurien Bay chronosequence, accounting for the disagreement with Hypothesis 1.

Is there a correlation or a trade-off between PPUE and P-remobilisation proficiency?

Species that were highly proficient at remobilising P (and thus had the lowest [P] in senesced leaves; Fig. 4) also exhibited the highest PPUE (Fig. 5B). This correlation is not simply due to leaves with a low mature leaf [P], and thus a high PPUE, inevitably also having a low senesced leaf [P], because the same correlation is not found for N. That is, leaves with a low mature leaf [N], and thus a high PNUE, do not have a low senesced leaf [N]. In highly P-efficient Proteaceae, a high PPUE is largely accounted for by functioning at very low levels of ribosomal RNA (rRNA) (Sulpice *et al.*, 2014), replacement of phospholipids by galactolipids and sulfolipids (Lambers *et al.*, 2012), and preferential allocation of P to mesophyll cells (Hayes *et al.*, 2018). For *Melaleuca systena*, there is evidence for a convergent P-investment pattern (Guilherme Pereira *et al.*, 2018, Li *et al.*, 2019), but there is no information for any of the other species. Our results support these findings and confirm Hypothesis 3, with PPUE being greater in the species that preferentially allocate P to mesophyll cells, rather than epidermal cells (Fig. 6). There is also evidence that preferential allocation of P to mesophyll cells allowed leaf P to be remobilised more proficiently. For example, *Templetonia retusa*, which preferentially allocates P to its upper epidermis (Guilherme Pereira *et al.*, 2018), showed a very low P-resorption proficiency. Further, Proteaceae species, which preferentially allocate P to their mesophyll (Hayes *et al.*, 2018), exhibited the highest P-remobilisation proficiencies (Fig. 7). It could be argued that the low mature leaf [P] of Proteaceae might account for this difference, but even with significantly lower leaf [P] (Fig. 6A), the species that allocated P to their mesophyll showed higher P-resorption efficiency (Fig. 6C). This suggests that the allocation of P to metabolically-active

tissues facilitates P resorption. So far, this information is merely correlative, and the exact mechanism for this, if any, is unknown; it is likely related to the presence of specific P transporters, phosphatases, and proximity to the phloem. Interestingly, variation in PNUE was not correlated with that in N-remobilisation proficiency (Fig. 5a). In the highly P-efficient Proteaceae, low rRNA levels are associated with low leaf [protein] and [N], and thus a high PNUE (Sulpice *et al.*, 2014). We surmise that selective pressures in severely P-impoverished landscapes are much stronger to remobilise P than to remobilise N, which is not the most limiting nutrient in ancient landscapes. Figure 7 indicates that these selective pressures were just as strong in non-Proteaceae as in Proteaceae, which exhibit a very high PPUE and remobilise P very efficiently (Denton *et al.*, 2007, Sulpice *et al.*, 2014).

Photosynthesis

Averaged area-based and mass-based rates of photosynthesis were similar at all sites (Fig. 3), unlike the continually declining trend found at the Franz Josef chronosequence in New Zealand, which is the only other chronosequence for which gas exchange data are available (Whitehead *et al.*, 2005). Thus, our results do not support Hypothesis 2 (i.e. that traits such as photosynthesis should exhibit a greater decline with increasing soil age than that seen at other chronosequences). At the oldest site along the Franz Josef chronosequence, rates declined from 16 µmol m^{-2} s^{-1} to about 4 µmol m^{-2} s^{-1}, whereas along the Jurien Bay chronosequence, with a much stronger decline in soil P availability, rates averaged at 17 µmol m^{-2} s^{-1}. It should be noted that all sites along the Jurien Bay chronosequence showed lower soil [P] than those along the Franz Josef chronosequence of similar age (Richardson *et al.*, 2004). This further highlights the extraordinary capacity of the Jurien Bay chronosequence species to maintain rapid rates of photosynthesis across some of the most P-impoverished soils found in terrestrial ecosystems. As we discuss below, this capacity to exhibit relatively rapid photosynthetic rates is not simply a result of the representative species all being members of the cluster-root forming Proteaceae.

South-western Australian Proteaceae in severely P-impoverished habitats exhibit a very high PPUE (Denton *et al.*, 2007, Lambers *et al.*, 2012). The high PPUE of Proteaceae is accounted for by: (1) preferential allocation of P to mesophyll cells, rather than epidermal cells (Hayes *et al.*, 2018, Shane *et al.*, 2004), as was thought to be common in most dicots (Conn & Gilliham, 2010); (2) extensive replacement of phospholipids by galactolipids and sulfolipids in mature leaves (Lambers *et al.*, 2012); functioning at very low levels of rRNA (Sulpice *et al.*, 2014). Importantly, however, the present results show that other species in different families on the oldest sites also show a very high PPUE, compared with species on the younger dunes. This differs markedly from what has been found along the Franz Josef chronosequence in New Zealand (Turnbull *et al.*, 2016, Whitehead *et al.*,

2005). It will be interesting to explore how species in other families achieve a high PPUE. We do know that they also preferentially allocate P to their mesophyll (Guilherme Pereira *et al.*, 2018), but have no information on the other two aspects, phospholipids and rRNA, except for *Melaleuca systena*, which shows a convergent pattern (Li *et al.*, 2019).

In addition to exhibiting high PPUE, species on the oldest dunes also showed a high PNUE (Fig. 3c). Using N efficiently (*i.e.* functioning at low leaf protein concentrations) reduces the amount of P required for rRNA, and thus increases P-use efficiency. This is most likely what drives this high N-use efficiency, because N is not a key limiting nutrient on the older dunes (Hayes *et al.*, 2014, Laliberté *et al.*, 2012), but N-use efficiency and P-use efficiency are tightly linked, via rRNA (Veneklaas *et al.*, 2012).

Respiration

Rates of respiration per unit leaf area, leaf mass, leaf N, and leaf P were relatively similar at all sites (Fig. 3); this pattern is quite different from that found at the Franz Josef chronosequence, where rates were faster at younger sites, and rates were also slower than the present values (Atkin *et al.*, 2013, Turnbull *et al.*, 2005). However, faster respiration rates at the older sites along the Jurien Bay chronosequence are to be expected, given faster rates of N- and P-based photosynthesis at these sites, contrary to the pattern along the Franz Josef chronosequence (Whitehead *et al.*, 2005).

The fraction of photosynthates used in leaf respiration - while differing among the sites - was largely independent of site age, indicating that leaf respiratory efficiency did not simply vary in response to soil age. In mature, fully expanded leaves that have a functioning photosynthetic apparatus, respiration is required to provide energy for export of sugars from the leaves via the phloem and for maintenance respiration (Bouma *et al.*, 1995). Since the ratio of respiration to photosynthesis did not systematically decline with increasing soil age, costs of phloem loading of sugars likely reflect rates of photosynthesis, which were independent of site age. However, maintenance costs, associated with slower protein turnover due to lower protein concentrations might be expected to decline (Bouma *et al.*, 1994), but this is not supported by the respiration rates that were independent of site age. Lower protein levels and slower rates of turnover imply a lower requirement for rRNA, a major P fraction in mature leaves (Veneklaas *et al.*, 2012). Proteaceae from south-western Australia in particular are known to operate at very low levels of rRNA, thus operating at a very high PPUE (Sulpice *et al.*, 2014). The present results on leaf respiration and PPUE suggest that other species on the most P-impoverished sites may also operate at low rRNA levels, but further research would need to test this hypothesis.

Conclusions

South-western Australia is one of the world's 35 biodiversity hotspots, with a myriad of species having adapted to soils containing extremely low [P] and [N]. Yet, variability in nutrient availability occurs, with species growing on young soils adjacent to the ocean exhibiting relatively high leaf [N] and [P]. Away from the ocean, soils have aged and soil and leaf nutrient concentrations declined markedly, with [P] being particularly low. Such changes might be expected to result in a concomitant decline in leaf photosynthesis and respiration rates. Yet, this does not occur, with leaves of plants growing on the oldest, most nutrient-impoverished soils exhibiting similar rates of CO_2 exchange as their counterparts growing on more nutrient-rich, younger soils. Plants growing on old soils also exhibit more efficient P resorption than their young-soil counterparts. Adaptations to acquire P from severely P-impoverished soils are common in Proteaceae and some Fabaceae, but they appear to be absent in all non-Proteaceae species in this study. However, adaptations at the leaf level appear to have converged, because our results show that non-Proteaceae species were also able to cope with very low P availability on old soils using similar leaf-level traits to those exhibited by Proteaceae. Determining the nature of the leaf-level processes that enable non-Proteaceae species to occupy sites of extreme low P availability remains a priority.

Acknowledgements

C.G.P and P.E.H were supported by Australian Government Research Training Program Scholarships supplemented by a top-up scholarship from the Australian Research Council (ARC; DP130100005). This research was supported by the Australian Research Council, DP0985685 and DP110101120 to HL, and DP0986823 to OKA. The authors acknowledge Nicolas Honvault for the SEM work and use of the facilities of the Australian Microscopy & Microanalysis Research Facility at the Centre for Microscopy, Characterisation & Analysis (CMCA), The University of Western Australia, a facility funded by the University, State and Commonwealth Governments. We also acknowledge the Department of Biodiversity, Conservation and Attractions (Western Australia) and Shires of Dandaragan, and Coorow for permission to conduct research on land under their administration.

Author contributions

O.S.O'S, L.K.W., H.L. and O.K.A. planned and designed the research. O.S.O'S, L.K.W., C.G.P., P.E.H. and P.L.C. performed experiments, conducted fieldwork, analysed data etc. H.L., O.K.A., C.G.P. and P.E.H. wrote the manuscript, with critical input from all others. C.G.P. and P.E.H. contributed equally. O.S.O'S and L.K.W. contributed equally.

Data Availability

Data available from the Dryad Digital Repository: https://doi.org/10.5061/dryad.sn1s14h (Atkin, 2019)

References

Albornoz, F.E., Burgess, T.I., Lambers, H., Etchells, H. & Laliberté, E. (2017) Native soil-borne pathogens equalise differences in competitive ability between plants of contrasting nutrient-acquisition strategies. *Journal of Ecology*, **105**, 549–557.

Allen, S.E., Grimshaw, H.M., Parkinson, J.A. & Quarmby, C. (1974) *Chemical Analysis of Ecological Materials*. Blackwell Scientific Publications, Oxford, UK.

Aplin, T.E.H. & Cannon, J.R. (1971) Distribution of alkaloids in some Western Australian plants. *Economic Botany*, **25**, 366-380.

Atkin, O.K. (2019). Data from: Trait convergence in photosynthetic nutrient-use efficiency along a 2-million year dune chronosequence in a global biodiversity hotspot. Dryad Digital Repository. doi:10.5061/dryad.sn1s14h

Atkin, O.K., Turnbull, M.H., Zaragoza-Castells, J., Fyllas, N.M., Lloyd, J., Meir, P. & Griffin, K.L. (2013) Light inhibition of leaf respiration as soil fertility declines along a post-glacial chronosequence in New Zealand: an analysis using the Kok method. *Plant and Soil*, **367**, 163-182.

Austin, A.T. & Vivanco, L. (2006) Plant litter decomposition in a semi-arid ecosystem controlled by photodegradation. *Nature*, **442**, 555-558.

Bates, D., Maechler, M., Bolker, B. & Walker, S. (2015) Fitting linear mixed-effects models using lme4. *Journal of Statistical Software*, **67**, 1-48.

Bermúdez-Torres, K., Martínez Herrera, J., Figueroa Brito, R., Wink, M. & Legal, L. (2009) Activity of quinolizidine alkaloids from three Mexican *Lupinus* against the lepidopteran crop pest *Spodoptera frugiperda*. *BioControl*, **54**, 459-466.

Bernasconi, S.M., Bauder, A., Bourdon, B., Brunner, I., Bünemann, E., Chris, I., Derungs, N., Edwards, P., Farinotti, D., Frey, B., Frossard, E., Furrer, G., Gierga, M., Göransson, H., Gülland, K., Hagedorn, F., Hajdas, I., Hindshaw, R., Ivy-Ochs, S., Jansa, J., Jonas, T., Kiczka, M., Kretzschmar, R., Lemarchand, E., Luster, J., Magnusson, J., Mitchell, E.a.D., Venterink, H.O., Plötze, M., Reynolds, B., Smittenberg, R.H., Stähli, M., Tamburini, F., Tipper, E.T., Wacker, L., Welc, M., Wiederhold, J.G., Zeyer, J., Zimmermann, S. & Zumsteg, A. (2011) Chemical and biological gradients along the Damma Glacier soil chronosequence, Switzerland. *Vadose Zone Journal*, **10**, 867-883.

Bouma, T.J., De Visser, R., Janssen , J.H.J.A., De Kock, M.J., Van Leeuwen, P.H. & Lambers, H. (1994) Respiratory energy requirements and rate of protein turnover *in vivo* determined by the use of an inhibitor of protein synthesis and a probe to assess its effect. *Physiologia Plantarum*, **92**, 585-594.

Bouma, T.J., De Visser, R., Van Leeuwen, P.H., De Kock, M.J. & Lambers, H. (1995) The respiratory energy requirements involved in nocturnal carbohydrate export from starch-storing mature source leaves and their contribution to leaf dark respiration. *Journal of Experimental Botany*, **46**, 1185-1194.

Conn, S. & Gilliham, M. (2010) Comparative physiology of elemental distributions in plants. *Annals of Botany*, **105**, 1081-1102.

Cordell, S., Goldstein, G., Meinzer, F.C. & Vitousek, P.M. (2001) Regulation of leaf life-span and nutrient-use efficiency of *Metrosideros polymorpha* trees at two extremes of a long chronosequence in Hawaii. *Oecologia*, **127**, 198-206.

Denton, M.D., Veneklaas, E.J., Freimoser, F.M. & Lambers, H. (2007) *Banksia* species (Proteaceae) from severely phosphorus-impoverished soils exhibit extreme efficiency in the use and re-mobilization of phosphorus. *Plant, Cell and Environment*, **30**, 1557-1565.

Dijkstra, P. (1998) Cause and effect of differences in SLA. In: *Causes and Consequences of Variation in Growth Rate and Productivity of Higher Plants* (ed Lambers, H., Cambridge, M.L., Konings, H., Pons, T.L.), pp. 125-140. SPB Academic Publishers, The Hague, the Netherlands.

Eger, A., Almond, P., Wells, A. & Condron, L. (2013) Quantifying ecosystem rejuvenation: foliar nutrient concentrations and vegetation communities across a dust gradient and a chronosequence. *Plant and Soil*, **367**, 93-109.

Evans, J.R. (1989) Photosynthesis and nitrogen relationships in leaves of C_3 plants. *Oecologia*, **78**, 9-19.

Evans, W.C. & Ramsey, K.P.A. (1983) Alkaloids of the Solanaceae tribe Anthocercideae. *Phytochemistry*, **22**, 2219-2225.

Evans, W.C. & Treagust, P.G. (1973) Distribution of alkaloids in *Anthocercis littorea* and *A. viscosa*. *Phytochemistry*, **12**, 2505-2507.

Evans, W.C. & Woolley, V.A. (1969) Biosynthesis of the (+)-2-hydroxy-3-phenylpropionic acid moiety of littorine in *Datura sanguinea* and *Anthocercis littorea*. *Phytochemistry*, **8**, 2183-2187.

Gliksman, D., Rey, A., Seligmann, R., Dumbur, R., Sperling, O., Navon, Y., Haenel, S., De Angelis, P., Arnone John, A. & Grünzweig José, M. (2016) Biotic degradation at night, abiotic degradation at day: positive feedbacks on litter decomposition in drylands. *Global Change Biology*, **23**, 1564-1574.

Guilherme Pereira, C., Clode, P.L., Oliveira, R.S. & Lambers, H. (2018) Eudicots from severely phosphorus-impoverished environments preferentially allocate phosphorus to their mesophyll. *New Phytologist*, **218**, 959-973.

Gundale, M.J., Fajardo, A., Lucas, R.W., Nilsson, M.-C. & Wardle, D.A. (2011) Resource heterogeneity does not explain the diversity–productivity relationship across a boreal island fertility gradient. *Ecography*, **34**, 887-896.

Hassiotou, F., Evans, J.R., Ludwig, M. & Veneklaas, E.J. (2009) Stomatal crypts may facilitate diffusion of CO_2 to adaxial mesophyll cells in thick sclerophylls. *Plant, Cell and Environment*, **32**, 1596-1611.

Hawkins, H.-J., Hettasch, H., Mesjasz-Przybylowicz, J., Przybylowicz, W. & Cramer, M.D. (2008) Phosphorus toxicity in the Proteaceae: a problem in post-agricultural lands. *Scientia Horticulturae*, **117**, 357-365.

Hayes, P., Turner, B.L., Lambers, H. & Laliberté, E. (2014) Foliar nutrient concentrations and resorption efficiency in plants of contrasting nutrient-acquisition strategies along a 2-million-year dune chronosequence. *Journal of Ecology*, **102**, 396-410.

Hayes, P.E., Clode, P.L., Oliveira, R.S. & Lambers, H. (2018) Proteaceae from phosphorus-impoverished habitats preferentially allocate phosphorus to photosynthetic cells: an adaptation improving phosphorus-use efficiency. *Plant, Cell and Environment*, **41**, 605–619.

Hopper, S.D. & Gioia, P. (2004) The Southwest Australian Floristic Region: evolution and conservation of a global hotspot of biodiversity. *Annual Review of Ecology, Evolution and Systematics*, **35**, 623-650.

Killingbeck, K.T. (1996) Nutrients in senesced leaves: keys to the search for potential resorption and resorption proficiency. *Ecology*, **77**, 1716-1727.

Kitayama, K., Mueller-Dombois, D. & Vitousek, P.M. (1995) Primary succession of Hawaiian montane rain forest on a chronosequence of eight lava flows. *Journal of Vegetation Science*, **6**, 211-222.

Kornfeld, A., Atkin, O.K., Griffin, K.L., Horton, T.W., Yakir, D. & Turnbull, M.H. (2013) Modulation of respiratory metabolism in response to nutrient changes along a soil chronosequence. *Plant, Cell and Environment*, **36**, 1120–1134.

Lagerström, A., Nilsson, M.-C. & Wardle, D. (2013) Decoupled responses of tree and shrub leaf and litter trait values to ecosystem retrogression across an island area gradient. *Plant and Soil*, **367**, 183-197

Laliberté, E., Grace, J.B., Huston, M.A., Lambers, H., Teste, F.P., Turner, B.L. & Wardle, D.A. (2013a) How does pedogenesis drive plant diversity? *Trends in Ecology & Evolution*, **28**, 331–340.

Laliberté, E., Turner, B.L., Costes, T., Pearse, S.J., Wyrwolll, K.-H., Zemunik, G. & Lambers, H. (2012) Experimental assessment of nutrient limitation along a 2-million year dune chronosequence in the south-western Australia biodiversity hotspot. *Journal of Ecology*, **100**, 631-642.

Laliberté, E., Turner, B.L., Zemunik, G., Wyrwoll, K.-H., Pearse, S.J. & Lambers, H. (2013b) Nutrient limitation along the Jurien Bay dune chronosequence: response to Uren & Parsons. *Journal of Ecology*, **101**, 1088-1092.

Lambers, H., ed (2014) *Plant Life on the Sandplains in Southwest Australia, a Global Biodiversity Hotspot*. University of Western Australia Publishing, Crawley, Australia.

Lambers, H., Albornoz, F., Kotula, L., Laliberté, E., Ranathunge, K., Teste, F.P. & Zemunik, G. (2018) How belowground interactions contribute to the coexistence of mycorrhizal and non-mycorrhizal species in severely phosphorus-impoverished hyperdiverse ecosystems. *Plant and Soil*, **424**, 11-34.

Lambers, H., Cawthray, G.R., Giavalisco, P., Kuo, J., Laliberté, E., Pearse, S.J., Scheible, W.-R., Stitt, M., Teste, F. & Turner, B.L. (2012) Proteaceae from severely phosphorus-impoverished soils extensively replace phospholipids with galactolipids and sulfolipids during leaf development to achieve a high photosynthetic phosphorus-use efficiency. *New Phytologist*, **196**, 1098-1108.

Lambers, H., Chapin, F.S. & Pons, T.L. (2008) *Plant Physiological Ecology, second edition*. Springer, New York.

Lambers, H., Clode, P.L., Hawkins, H.-J., Laliberté, E., Oliveira, R.S., Reddell, P., Shane, M.W., Stitt, M. & Weston, P. (2015) Metabolic adaptations of the non-mycotrophic Proteaceae to soil with a low phosphorus availability. In: *Annual Plant Reviews, Volume 48, Phosphorus Metabolism in Plants* (eds Plaxton, W.C. & Lambers , H.), pp. 289-336. John Wiley & Sons, Chicester.

Lambers, H. & Poorter, H. (1992) Inherent variation in growth rate between higher plants: a search for physiological causes and ecological consequences. *Advances in Ecological Research*, **22**, 187-261.

Lambers, H., Shane, M.W., Laliberté, E., Swarts, N.D., Teste, F.P. & Zemunik, G. (2014) Plant mineral nutrition. In: *Plant Life on the Sandplains in Southwest Australia, a Global Biodiversity Hotspot* (ed Lambers, H.), pp. 101-127. UWA Publishing, Crawley.

Legendre, P. (2011) *lmodel2: Model II Regression. R package version 1.7-1/r1794*.

Li, Y., Zhang, X., Han, Z., Lambers, H. & Finnegan, P.M. (2019) Leaf phosphorus fractions in species with contrasting strategies as dependent on soil phosphorus concentrations along the Jurien Bay chronosequence. *New Phytologist*, under review.

733 Motomizu, S., Wakimoto, T. & Toei, K. (1983) Spectrophotometric determination of phosphate in
734 river waters with molybdate and malachite green. *Analyst*, **108**, 361-367.
735 Myers, N., Mittermeier, R.A., Mittermeier, C.G., Da Fonseca, G.a.B. & Kent, J. (2000) Biodiversity
736 hotspots for conservation priorities. *Nature*, **403**, 853-858.
737 Pate, J.S., Casson, N.E., Rullo, J. & Kuo, J. (1985) Biology of fire ephemerals of the sandplains of the
738 kwongan of south-western Australia. *Functional Plant Biology*, **12**, 641-655.
739 Peltzer, D., Wardle, D., Allison, V., Baisden, W., Bardgett, R., Chadwick, O., Condron, L., Parfitt, R.,
740 Porder, S., Richardson, S., Turner, B., Vitousek, P., Walker, J. & Walker, L. (2010)
741 Understanding ecosystem retrogression. *Ecological Monographs*, **80**, 509-529.
742 Pérez, C.A., Aravena, J.C., Silva, W.A., Mcculloch, R., Armesto, J.J. & Parfitt, R. (2016) Patterns of
743 ecosystem development in glacial foreland chronosequences: a comparative analysis of Chile
744 and New Zealand. *New Zealand Journal of Botany*, **54**, 156–174.
745 Png, G.K., Turner, B.L., Albornoz, F.E., Hayes, P.E., Lambers, H. & Laliberté, E. (2017) Greater root
746 phosphatase activity in nitrogen-fixing rhizobial but not actinorhizal plants with declining
747 phosphorus availability. *Journal of Ecology*, **105**, 1246–1255.
748 Powell, J.R., Karunaratne, S., Campbell, C.D., Yao, H., Robinson, L. & Singh, B.J. (2015) Deterministic
749 processes vary during community assembly for ecologically dissimilar taxa. . *Nature*
750 *Communications*, **6**, 8444.
751 Prietzel, J., Dümig, A., Wu, Y., Zhou, J. & Klysubun, W. (2013) Synchrotron-based P K-edge XANES
752 spectroscopy reveals rapid changes of phosphorus speciation in the topsoil of two glacier
753 foreland chronosequences. *Geochimica et Cosmochimica Acta*, **108**, 154-171.
754 Richardson, S., Peltzer, D., Allen, R., Mcglone, M. & Parfitt, R. (2004) Rapid development of
755 phosphorus limitation in temperate rainforest along the Franz Josef soil chronosequence.
756 *Oecologia*, **139**, 267-276.
757 Richardson, S.J., Peltzer, D.A., Allen, R.B. & Mcglone, M.S. (2010) Declining soil fertility does not
758 increase leaf lifespan within species: evidence from the Franz Josef chronosequence, New
759 Zealand. *New Zealand Journal of Ecology*, **34**, 306-310.
760 Shane, M.W., Mccully, M.E. & Lambers, H. (2004) Tissue and cellular phosphorus storage during
761 development of phosphorus toxicity in *Hakea prostrata* (Proteaceae). *Journal of*
762 *Experimental Botany*, **55**, 1033-1044.
763 Stevens, P.R. & Walker, T.W. (1970) The chronosequence concept and soil formation. *Quarterly*
764 *Review of Biology*, **45**, 333-350.
765 Sulpice, R., Ishihara, H., Schlereth, A., Cawthray, G.R., Encke, B., Giavalisco, P., Ivakov, A., Arrivault,
766 S., Jost, R., Krohn, N., Kuo, J., Laliberté, E., Pearse, S.J., Raven, J.A., Scheible, W.R., Teste, F.,

767 Veneklaas, E.J., Stitt, M. & Lambers, H. (2014) Low levels of ribosomal RNA partly account for
768 the very high photosynthetic phosphorus-use efficiency of Proteaceae species. *Plant, Cell*
769 *and Environment*, **37**, 1276-1298.
770 Teste, F.P., Kardol, P., Turner, B.L., Wardle, D.A., Zemunik, G., Renton, M. & Laliberté, E. (2017) Plant-
771 soil feedback and the maintenance of diversity in Mediterranean-climate shrublands.
772 *Science*, **355**, 173-176.
773 Turnbull, M.H., Griffin, K.L., Fyllas, N.M., Lloyd, J., Meir, P. & Atkin, O.K. (2016) Separating species
774 and environmental determinants of leaf functional traits in temperate rainforest plants
775 along a soil-development chronosequence. *Functional Plant Biology*, **43,** , 751–765.
776 Turnbull, M.H., Tissue, D.T., Griffin, K.L., Richardson, S.J., Peltzer, D.A. & Whitehead, D. (2005)
777 Respiration characteristics in temperate rainforest tree species differ along a long-term soil-
778 development chronosequence. *Oecologia*, **143**, 271-279.
779 Turner, B.L. & Condron, L.M. (2013) Pedogenesis, nutrient dynamics, and ecosystem development:
780 the legacy of T.W. Walker and J.K. Syers. *Plant and Soil*, **367**, 1-10.
781 Turner, B.L. & Laliberté, E. (2015) Soil development and nutrient availability along a 2 million-year
782 coastal dune chronosequence under species-rich Mediterranean shrubland in southwestern
783 Australia. *Ecosystems*, **18**, 287-309.
784 Turner, B.L., Laliberté, E. & Hayes, P.E. (2018) A climosequence of chronosequences in southwestern
785 Australia. *European Journal of Soil Science*, **69**, 69-85.
786 Veneklaas, E.J., Lambers, H., Bragg, J., Finnegan, P.M., Lovelock, C.E., Plaxton, W.C., Price, C.,
787 Scheible, W.-R., Shane, M.W., White, P.J. & Raven, J.A. (2012) Opportunities for improving
788 phosphorus-use efficiency in crop plants. *New Phytologist*, **195**, 306-320.
789 Veneklaas, E.J. & Poot, P. (2003) Seasonal patterns in water use and leaf turnover of different plant
790 functional types in a species-rich woodland, south-western Australia. *Plant and Soil*, **257**,
791 295-304.
792 Vile, D., Garnier, E., Shipley, B., Laurent, G., Navas, M.L., Roumet, C., Lavorel, S., Diaz, S., Hodgson,
793 J.G., Lloret, F., Midgley, G.F., Poorter, H., Rutherford, M.C., Wilson, P.J. & Wright, I.J. (2005)
794 Specific leaf area and dry matter content estimate thickness in laminar leaves. *Annals of*
795 *Botany*, **96**, 1129-1136.
796 Vitousek, P.M., Walker, L.R., Whiteaker, L.D. & Matson, P.A. (1993) Nutrient limitations to plant
797 growth during primary succession in Hawaii Volcanoes National Park. *Biogeochemistry*, **23**,
798 197-215.
799 Walker, T.W. & Syers, J.K. (1976) The fate of phosphorus during pedogenesis. *Geoderma*, **15**, 1-9.

Wardle, D.A., Walker, L.R. & Bardgett, R.D. (2004) Ecosystem properties and forest decline in contrasting long-term chronosequences. *Science*, **305**, 509-513.

Whitehead, D., Boelman, N.T., Turnbull, M.H., Griffin, K.L., Tissue, D.T., Barbour, M.M., Hunt, J.E., Richardson, S.J. & Peltzer, D.A. (2005) Photosynthesis and reflectance indices for rainforest species in ecosystems undergoing progression and retrogression along a soil fertility chronosequence in New Zealand. *Oecologia*, **144**, 233-244.

Witkowski, E.T.F. & Lamont, B.B. (1991) Leaf specific mass confounds leaf density and thickness. *Oecologia*, **88**, 486-493.

Wright, I.J., Reich, P.B., Westoby, M., Ackerly, D.D., Baruch, Z., Bongers, F., Cavender-Bares, J., Chapin, T., Cornelissen, J.H.C., Diemer, M., Flexas, J., Garnier, E., Groom, P.K., Gulias, J., Hikosaka, K., Lamont, B.B., Lee, T., Lee, W., Lusk, C., Midgley, J.J., Navas, M.-L., Niinemets, Ü., Oleksyn, J., Osada, N., Poorter, H., Poot, P., Prior, L., Pyankov, V.I., Roumet, C., Thomas, S.C., Tjoelker, M.G., Veneklaas, E.J. & Villar, R. (2004) The worldwide leaf economics spectrum. *Nature*, **428**, 821-827.

Wyrwoll, K.-H., Turner, B.L. & Findlater, P. (2014) On the origins, geomorphology and soils of the sandplains of south-western Australia. In: *Plant Life on the Sandplains in Southwest Australia, a Global Biodiversity Hotspot* (ed Lambers , H.), pp. 3-22. UWA Publishing, Crawley.

Zemunik, G., Turner, B.L., Lambers, H. & Laliberté, E. (2015) Diversity of plant nutrient-acquisition strategies increases during long-term ecosystem development. *Nature Plants*, **1**, 10.1038/nplants.2015.1050.

Zemunik, G., Turner, B.L., Lambers, H. & Laliberté, E. (2016) Increasing plant species diversity and extreme species turnover accompany declining soil fertility along a long-term chronosequence in a biodiversity hotspot. *Journal of Ecology*, **104**, 792-805.

Zhou, J., Bing, H., Wu, Y., Yang, Z., Wang, J., Sun, H., Luo, J. & Liang, J. (2016) Rapid weathering processes of a 120-year-old chronosequence in the Hailuogou Glacier foreland, Mt. Gongga, SW China. *Geoderma*, **267**, 78-91.

Zhou, J., Wu, Y., Prietzel, J., Bing, H., Yu, D., Sun, S., Luo, J. & Sun, H. (2013) Changes of soil phosphorus speciation along a 120-year soil chronosequence in the Hailuogou Glacier retreat area (Gongga Mountain, SW China). *Geoderma*, **195–196**, 251-259.

Table 1. Mean (± s.e., *n* = 3-10) values of leaf dry mass per unit leaf area (LMA), leaf fresh mass per unit leaf area (FMA), leaf dry matter content (DMC), leaf nitrogen (N) concentration, leaf phosphorus (P) concentration, and leaf N to P concentration (N:P ratio) for different plant species within three stages of the Jurien Bay dune chronosequence. Stage 1 refers to the progressive phase of very young dunes, where plant growth is limited by N; stage 3 represents the retrogressive phase of intermediate-aged dunes, where plant productivity is co-limited by N and P; while stage 4 represents old dunes, where P is the main macronutrient limiting plant productivity.

Stage	Species	Plant Family	LMA (g m^{-2})	FMA (g m^{-2})	DMC (%)	N (mg g^{-1})	P (mg g^{-1})	N:P ratio
1	*Acacia rostellifera* Benth.	Fabaceae	136 ± 40	492 ± 15	0.28 ± 0.09	19.7 ± 2.6	1.04 ± 0.10	18.8 ± 2.5
	Anthocercis littorea Labill.	Solanaceae	137 ± 19	849 ± 45	0.16 ± 0.01	18.6 ± 2.4	-	-
	Dioscorea hastifolia Endl.	Dioscoreaceae	87 ± 7	351 ± 24	0.25 ± 0.01	17.7 ± 1.5	-	-
	Myoporum insulare R.Br.	Scrophulariaceae	137 ± 8	759 ± 40	0.18 ± 0.01	17.8 ± 0.8	2.09 ± 0.59	8.5 ± 0.4
	Olearia axillaris (DC.) Benth.	Asteraceae	172 ± 19	493 ± 38	0.35 ± 0.01	16.7 ± 1.1	1.41 ± 0.26	11.9 ± 0.8
	Spyridium globulosum (Labill.) Benth.	Rhamnaceae	164 ± 11	397 ± 22	0.41 ± 0.01	12.1 ± 0.5	0.47 ± 0.04	25.7 ± 1.1
	Templetonia retusa (Vent.) R.Br.	Fabaceae	172 ± 15	411 ± 15	0.42 ± 0.02	17.1 ± 1.5	0.86 ± 0.11	20.0 ± 1.7
3	*Acacia lasiocarpa* Benth.	Fabaceae	175 ± 18	627 ± 48	0.28 ± 0.02	18.6 ± 1.2	0.36 ± 0.05	51.1 ± 3.4
	Acacia rostellifera Benth.	Fabaceae	126 ± 5	425 ± 14	0.30 ± 0.01	19.8 ± 1.3	0.76 ± 0.05	26.1 ± 1.7
	Banksia nivea Labill.	Proteaceae	245 ± 11	532 ± 14	0.46 ± 0.02	7.0 ± 0.3	0.32 ± 0.05	22.1 ± 1.0
	Clematis linearifolia Steud.	Ranunculaceae	177 ± 5	591 ± 21	0.30 ± 0.01	19.7 ± 2.6	-	-
	Melaleuca systena Craven	Myrtaceae	178 ± 7	720 ± 52	0.25 ± 0.01	12.0 ± 0.7	0.47 ± 0.04	25.8 ± 1.5
	Opercularia spermacocea Juss.	Rubiaceae	124 ± 3	739 ± 7	0.17 ± 0.00	12.9 ± 0.2	-	-
	Phyllanthus calycinus Labill.	Phyllanthaceae	98 ± 5	331 ± 12	0.30 ± 0.02	15.2 ± 4.0	0.37 ± 0.02	40.6 ± 10.8
	Spyridium globulosum (Labill.) Benth.	Rhamnaceae	174 ± 9	377 ± 9	0.46 ± 0.02	11.5 ± 0.3	0.37 ± 0.01	31.2 ± 0.7
4	*Acacia rostellifera* Benth.	Fabaceae	155 ± 4	592 ± 30	0.26 ± 0.01	18.1 ± 1.2	0.46 ± 0.01	39.6 ± 2.5
	Anthocercis littorea Labill.	Solanaceae	114 ± 6	741 ± 42	0.16 ± 0.01	16.5 ± 2.0	-	-
	Banksia leptophylla var. *melletica* A.S.George	Proteaceae	161 ± 14	353 ± 22	0.46 ± 0.05	7.0 ± 0.7	0.38 ± 0.04	18.2 ± 1.7
	Banksia nivea Labill.	Proteaceae	300 ± 25	564 ± 24	0.53 ± 0.02	6.6 ± 0.2	0.34 ± 0.02	19.5 ± 0.5
	Banksia prionotes Lindl.	Proteaceae	225 ± 7	430 ± 8	0.52 ± 0.01	11.1 ± 0.8	0.34 ± 0.01	32.4 ± 2.2
	Conospermum stoechadis Endl.	Proteaceae	243 ± 31	747 ± 15	0.33 ± 0.04	9.5 ± 0.6	0.41 ± 0.03	23.1 ± 1.6
	Hakea incrassata R.Br.	Proteaceae	308 ± 13	674 ± 20	0.46 ± 0.01	5.7 ± 0.1	0.27 ± 0.02	20.9 ± 0.4
	Labichea cassioides DC.	Fabaceae	217 ± 32	478 ± 71	0.46 ± 0.02	12.0 ± 1.5	0.32 ± 0.02	37.3 ± 4.7
	Melaleuca systena Craven	Myrtaceae	295 ± 35	786 ± 69	0.37 ± 0.02	9.3 ± 0.8	-	-

Scaevola crassifolia Labill.	Goodeniaceae	136 ± 12	517 ± 30	0.26 ± 0.01	14.8 ± 0.5	-	-

856

857

Table 2. Mean (± s.e., n = 3-8) values of area-based and dry mass-based rates of CO_2 assimilation at 1800 µmol photons m^{-2} s^{-1} / 400 µmol mol^{-1} [CO_2] ($A_{sat,a}$ and $A_{sat,m}$, respectively), area-based and dry mass-based rates of CO_2 assimilation at 1800 µmol photons m^{-2} s^{-1} / 1500 µmol mol^{-1} [CO_2] ($A_{max,a}$ and $A_{max,m}$, respectively), area-based and dry mass-based rates of leaf respiration in the darkness ($R_{d,,a}$ and $R_{d,m}$, respectively), ratios of leaf respiration (R_d) to CO_2 assimilation rate at 1800 µmol photons m^{-2} s^{-1} / 400 µmol mol^{-1} [CO_2] (A_{sat}), and to CO_2 assimilation rate at 1800 µmol photons m^{-2} s^{-1} / 1500 µmol mol^{-1} [CO_2] (A_{max}). Note that A_{sat} is A_{net} under saturating irradiance and ambient CO_2, whilst A_{max} is A_{net} under saturating irradiance and elevated CO_2.

Stage	Species	$A_{sat,a}$ (µmol CO_2 m^{-2} s^{-1})	$A_{sat,m}$ (nmol CO_2 g^{-1} s^{-1})	$A_{max,a}$ (µmol CO_2 m^{-2} s^{-1})	$A_{max,m}$ (nmol CO_2 g^{-1} s^{-1})	$R_{d,a}$ (µmol CO_2 m^{-2} s^{-1})	$R_{d,m}$ (nmol CO_2 g^{-1} s^{-1})	R_d/A_{sat}	R_d/A_{max}
1	*Acacia rostellifera* Benth.	17.8 ± 1.9	188 ± 98	35 ± 2	342 ± 144	3.5 ± 1.0	42 ± 285	0.19 ± 0.04	0.10 ± 0.03
	Anthocercis littorea Labill.	13.9 ± 2.4	126 ± 34	27 ± 0.4	238 ± 32	1.7 ± 0.2	13 ± 2	0.11 ± 0.01	0.06 ± 0.01
	Dioscorea hastifolia Endl.	11.3 ± 1.8	1339 ± 22	25 ± 2	289 ± 39	1.2 ± 0.1	14 ± 3	0.11 ± 0.01	0.05 ± 0.00
	Myoporum insulare R.Br.	14.5 ± 1.7	106 ± 14	31 ± 2	231 ± 26	2.6 ± 0.3	20 ± 2	0.16 ± 0.02	0.07 ± 0.01
	Olearia axillaris (DC.) Benth.	13.7 ± 1.7	83 ± 15	28 ± 3	167 ± 23	4.2 ± 0.4	25 ± 0.6	0.32 ± 0.05	0.15 ± 0.02
	Spyridium globulosum (Labill.) Benth.	17.0 ± 2.0	102 ± 11	34 ± 4	206 ± 24	1.8 ± 0.2	11 ± 1	0.11 ± 0.01	0.06 ± 0.00
	Templetonia retusa (Vent.) R.Br.	13.7 ± 1.7	82 ± 13	31 ± 4	184 ± 26	1.6 ± 0.1	9 ± 1	0.14 ± 0.02	0.06 ± 0.01
3	*Acacia lasiocarpa* Benth.	26.7 ± 4.2	162 ± 37	58 ± 6	343 ± 55	8.4 ± 1.8	51 ± 16	0.34 ± 0.08	0.16 ± 0.04
	Acacia rostellifera Benth.	18.6 ± 0.7	148 ± 11	37 ± 2	290 ± 6	1.8 ± 0.2	15 ± 3	0.10 ± 0.01	0.05 ± 0.01
	Banksia nivea Labill.	15.5 ± 2.3	65 ± 9	40 ± 6	169 ± 19	1.6 ± 0.2	6 ± 0.8	0.10 ± 0.02	0.04 ± 0.01
	Clematis linearifolia Steud.	23.2 ± 2.9	131 ± 16	41 ± 8	234 ± 47	2.6 ± 0.7	14 ± 4	0.12 ± 0.05	0.08 ± 0.04
	Melaleuca systena Craven	14.5 ± 1.6	82 ± 10	39 ± 1	216 ± 5	6.1 ± 0.8	34 ± 5	0.44 ± 0.09	0.16 ± 0.02
	Opercularia spermacocea Juss.	22.8 ± 3.5	183 ± 25	42 ± 5	341 ± 33	2.7 ± 0.2	22 ± 1	0.13 ± 0.02	0.07 ± 0.01
	Phyllanthus calycinus Labill.	10.0 ± 0.8	103 ± 10	29 ± 3	293 ± 29	1.1 ± 0.2	12 ± 2	0.12 ± 0.03	0.04 ± 0.01
	Spyridium globulosum (Labill.) Benth.	17.8 ± 0.9	103 ± 2.6	38 ± 2	219 ± 9	1.2 ± 0.3	7 ± 2	0.07 ± 0.01	0.03 ± 0.01
4	*Acacia rostellifera* Benth.	23.9 ± 4.0	153 ± 23	49 ± 11	312 ± 63	3.3 ± 0.1	21 ± 0.5	0.15 ± 0.02	0.07 ± 0.01
	Anthocercis littorea Labill.	15.2 ± 2.7	134 ± 24	32 ± 0.3	285 ± 20	2.2 ± 0.3	19 ± 3	0.13 ± 0.02	0.07 ± 0.01
	Banksia leptophylla var. *melletica*	6.5 ± 1.2	40 ± 5	13 ± 1	81 ± 7	3.1 ± 0.3	20 ± 4	0.55 ± 0.14	0.25 ± 0.04
	Banksia nivea Labill.	23.0 ± 3.5	77 ± 11	41 ± 7	140 ± 27	1.7 ± 0.1	6 ± 0.7	0.08 ± 0.01	0.05 ± 0.01
	Banksia prionotes Lindl.	23.1 ± 1.0	102 ± 2	42 ± 3	188 ± 11	1.3 ± 0.0	6 ± 0.2	0.06 ± 0.00	0.03 ± 0.00
	Conospermum stoechadis Endl.	14.3 ± 3.3	68 ± 26	25 ± 5	106.3 ± 13.4	3.0 ± 0.2	13 ± 3	0.23 ± 0.04	0.13 ± 0.02
	Hakea incrassata R.Br.	15.0 ± 1.2	49 ± 3	32 ± 2	105 ± 5	2.4 ± 0.2	8 ± 0.4	0.16 ± 0.02	0.08 ± 0.01

	Labichea cassioides DC.	14.9 ± 3.3	78 ± 24	30 ± 6	157 ± 46	3.1 ± 0.3	16 ± 4	0.23 ± 0.04	0.11 ± 0.02
	Melaleuca systena Craven	23.9 ± 4.2	79 ± 5	47 ± 8	156 ± 11	5.0 ± 1.0	17 ± 2	0.21 ± 0.03	0.11 ± 0.01
	Scaevola crassifolia Labill.	16.4 ± 2.1	120± 12	37 ± 2	276 ± 9	2.3 ± 0.2	17 ± 1	0.14 ± 0.02	0.06 ± 0.00

Table 3. Mean (± s.e., n = 3-8) values of nitrogen and phosphorus-based rates of CO_2 assimilation at 1800 µmol photons m^{-2} s^{-1} PPFD / 400 µmol mol^{-1} [CO_2] ($PNUE_{sat}$ and $PPUE_{sat}$, respectively), nitrogen and phosphorus-based rates of CO_2 assimilation at 1800 µmol photons m^{-2} s^{-1} PPFD/1500 µmol mol^{-1} [CO_2] ($PNUE_{max}$ and $PPUE_{max}$, respectively), and nitrogen and phosphorus-based rates of leaf respiration in the darkness ($R_{d,N}$ and $R_{d,P}$, respectively).

Stage	Species	$PNUE_{sat}$ (µmol CO_2 g^{-1} N s^{-1})	$PPUE_{sat}$ (µmol CO_2 g^{-1} P s^{-1})	$PNUE_{max}$ (µmol CO_2 g^{-1} N s^{-1})	$PPUE_{max}$ (µmol CO_2 g^{-1} P s^{-1})	$R_{d,N}$ (µmol CO_2 g^{-1} N s^{-1})	$R_{d,P}$ (µmol CO_2 g^{-1} P s^{-1})
1	*Acacia rostellifera* Benth.	8.7 ± 3.5	181 ± 94	16.4 ± 4.8	328 ± 138	1.9 ± 1.0	39.8 ± 26.4
	Anthocercis littorea Labill.	5.8 ± 1.2	-	11.2 ± 0.3	-	0.7 ± 0.1	-
	Dioscorea hastifolia Endl.	7.4 ± 0.6	-	16.2 ± 1.1	-	0.8 ± 0.1	-
	Myoporum insulare R.Br.	6.0 ± 0.7	51 ± 7	13.1 ± 1.5	110 ± 12	1.1 ± 0.1	9.4 ± 0.9
	Olearia axillaris (DC.) Benth.	5.0 ± 0.8	59 ± 11	10.0 ± 1.1	119 ± 16	1.5 ± 0.1	17.5 ± 0.5
	Spyridium globulosum (Labill.) Benth.	8.6 ± 1.1	217 ± 24	17.4 ± 2.5	437 ± 52	0.9 ± 0.1	22.8 ± 2.2
	Templetonia retusa (Vent.) R.Br.	4.8 ± 0.5	96 ± 15	10.8 ± 1.0	215 ± 30	0.6 ± 0.0	10.9 ± 1.6
3	*Acacia lasiocarpa* Benth.	8.4 ± 1.4	445 ± 102	18.1 ± 1.8	941 ± 152	2.7 ± 0.7	139.8 ± 42.4
	Acacia rostellifera Benth.	7.6 ± 0.7	196 ± 14	14.8 ± 0.7	383 ± 8	0.7 ± 0.1	19.2 ± 3.3
	Banksia nivea Labill.	8.9 ± 1.1	205 ± 27	23.0 ± 1.7	530 ± 58	0.9 ± 0.1	20.2 ± 2.5
	Clematis linearifolia Steud.	6.7 ± 0.5	-	11.6 ± 1.2	-	0.8 ± 0.3	-
	Melaleuca systena Craven	6.9 ± 0.9	176 ± 21	18.0 ± 0.7	463 ± 10	2.8 ± 0.3	73.5 ± 10.3
	Opercularia spermacocea Juss.	14.2 ± 1.9	-	26.5 ± 2.5	-	1.7 ± 0.1	-
	Phyllanthus calycinus Labill.	7.7 ± 1.4	275 ± 28	22.4 ± 4.7	781 ± 78	0.8 ± 0.2	31.2 ± 6.4
	Spyridium globulosum (Labill.) Benth.	8.9 ± 0.3	277 ± 7	19.0 ± 0.9	591 ± 23	0.6 ± 0.1	18.8 ± 3.9
4	*Acacia rostellifera* Benth.	8.4 ± 1.0	334 ± 50	17.2 ± 3.2	681 ± 138	1.2 ± 0.0	46.2 ± 1.2
	Anthocercis littorea Labill.	7.9 ± 0.4	-	17.9 ± 2.4	-	1.1 ± 0.1	-
	Banksia leptophylla var. *melletica*	6.0 ± 1.2	104 ± 12	12.0 ± 1.6	211 ± 19	2.9 ± 0.3	52.7 ± 9.3
	Banksia nivea Labill.	11.5 ± 1.4	226 ± 31	21.2 ± 3.9	415 ± 79	0.9 ± 0.1	16.6 ± 2.0
	Banksia prionotes Lindl.	9.3 ± 0.5	299 ± 7	17.0 ± 1.1	547 ± 33	0.6 ± 0.0	17.7 ± 0.7

Conospermum stoechadis Endl.	6.7 ± 2.1	164 ± 63	11.0 ± 1.4	258 ± 32	1.4 ± 0.2	32.6 ± 6.6
Hakea incrassata R.Br.	8.6 ± 0.7	179 ± 12	18.4 ± 0.9	384 ± 19	1.4 ± 0.1	28.6 ± 1.6
Labichea cassioides DC.	6.3 ± 1.6	244 ± 74	12.7 ± 3.3	490 ± 144	1.3 ± 0.3	49.1 ± 11.3
Melaleuca systena Craven	8.7 ± 0.8	-	17.0 ± 0.8	-	1.8 ± 0.2	-
Scaevola crassifolia Labill.	8.2 ± 1.1	-	18.7 ± 0.8	-	1.1 ± 0.1	-

867

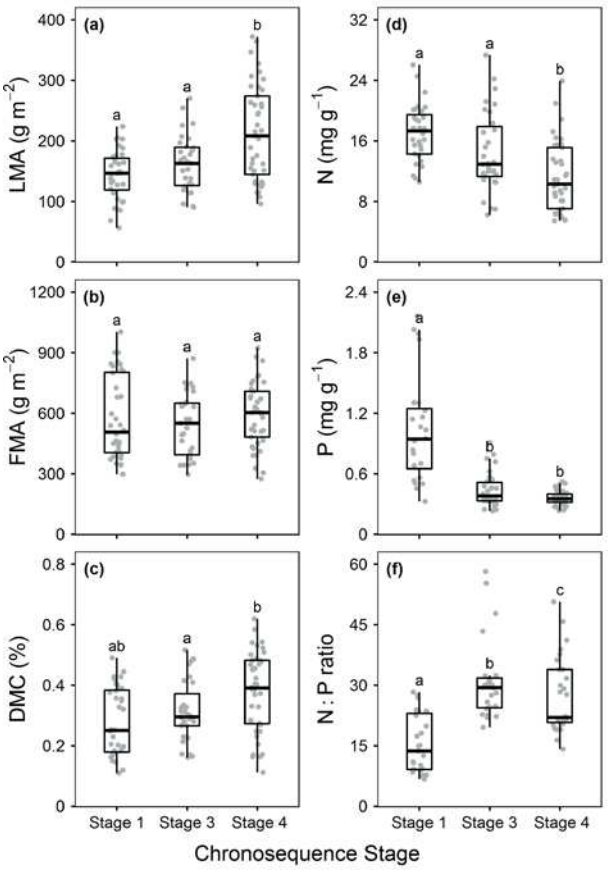

Figure 1. Leaf trait data for species in different soil development stages across the Jurien Bay dune chronosequence: (a) leaf mass per area (LMA); (b) fresh mass per area (FMA); (c) dry matter content (DMC); (d) leaf nitrogen concentration (N); (e) leaf phosphorus concentration (P) and; (f) leaf nitrogen to leaf phosphorus concentrations (N:P ratio). Box-plots with medians, 25th and 75th percentiles. Whiskers extend to 1.5 times the interquartile range. Data presented beyond whiskers represent outliers. Different letters indicate significant differences (P<0.05) among stages within each panel, based on Tukey`s HSD test

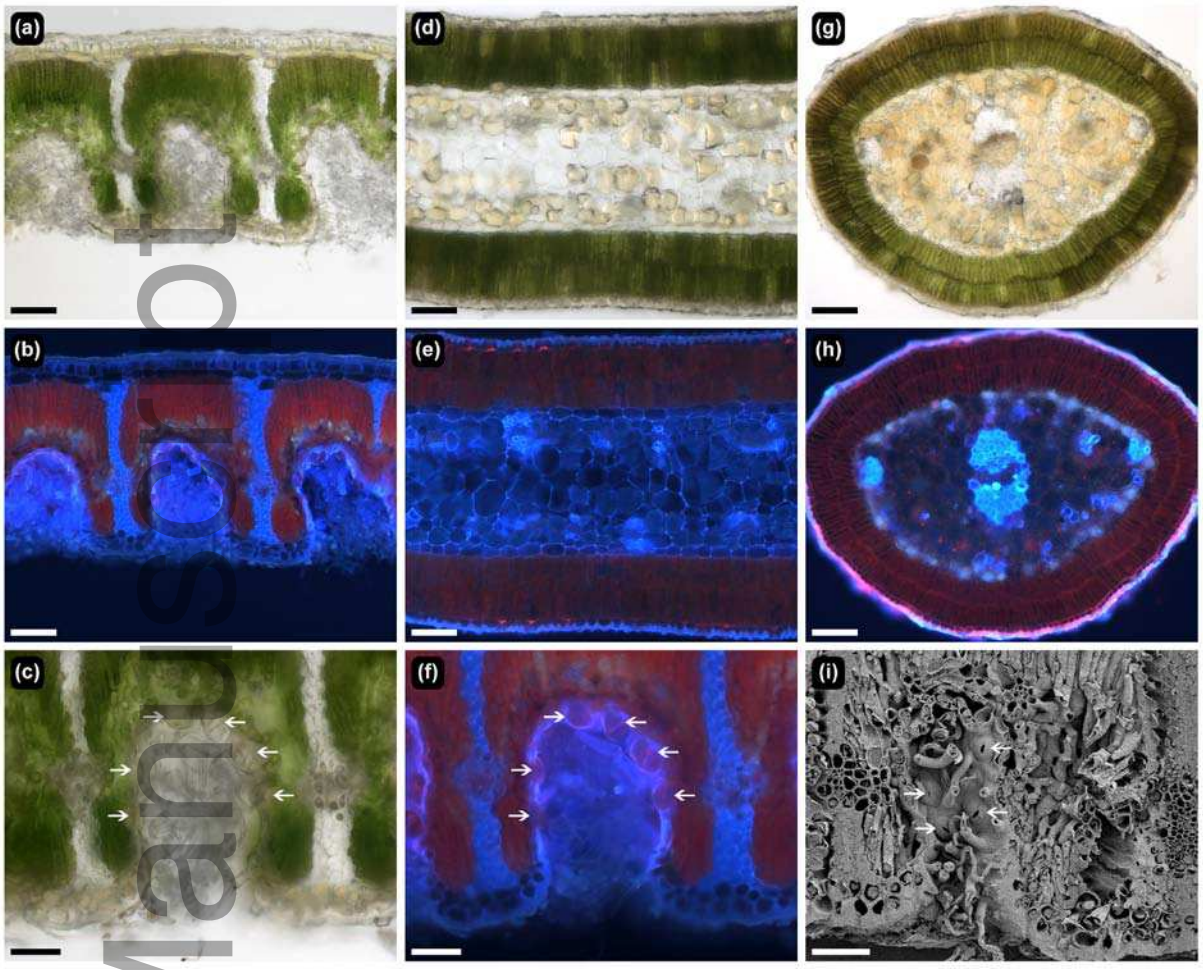

Figure 2. Cross sections of leaves collected along the Jurien Bay dune chronosequence. Leaves of *Banksia prionotes* viewed under brightfield (a) and fluorescence (b), with sunken stomata (white arrows) evident in stomatal crypts using brightfield (c), fluorescence (f), and scanning electron microscopy (i). Isobilateral phyllodes of *Acacia rostellifera* viewed under brightfield (d) and fluorescence (e). Ellipsoid leaves of *Melaleuca systena* viewed under brightfield (g) and fluorescence (h). Scale bars are 100 µm (a, b, d, e, g, h) and 50 µm (c, f, i).

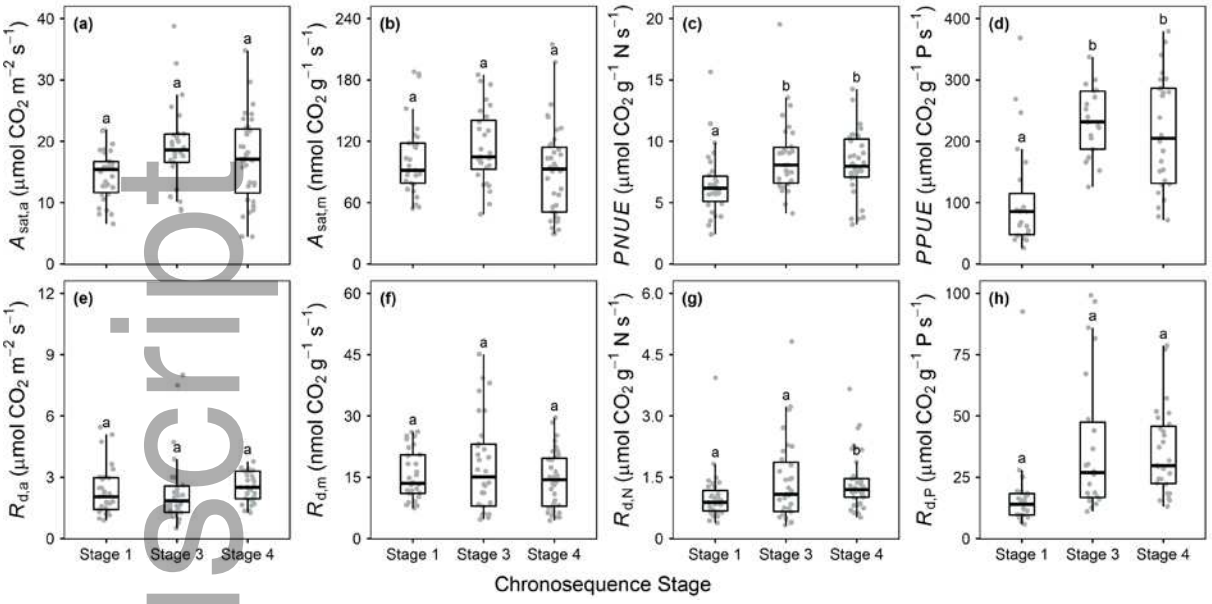

Figure 3. Saturated gas-exchange data for species in different soil development stages across the Jurien Bay chronosequence: (**a**) area-based rates of CO_2 assimilation ($A_{sat,a}$); (**b**) dry mass-based rates of CO_2 assimilation ($A_{sat,m}$); (**c**) nitrogen-based rates of CO_2 assimilation (*PNUE*); (**d**) phosphorus-based rates of CO_2 assimilation (*PPUE*); (**e**) area-based rates of dark respiration ($R_{d,a}$); (**f**) dry mass-based rates of dark respiration ($R_{d,m}$); (**g**) nitrogen-based rates of dark respiration ($R_{d,N}$) and; (**h**) phosphorus-based rates of dark respiration ($R_{d,P}$). Box-plots with medians, 25th and 75th percentiles. Whiskers extend to 1.5 times the interquartile range. Data presented beyond whiskers represent outliers. Different letters indicate significant differences (P<0.05) among stages within each panel, based on Tukey`s HSD test. All gas-exchange measurements were performed at 400 µmol mol^{-1} [CO_2], with 1800 µmol photons m^{-2} s^{-1} PPFD for the photosynthetic measurements.

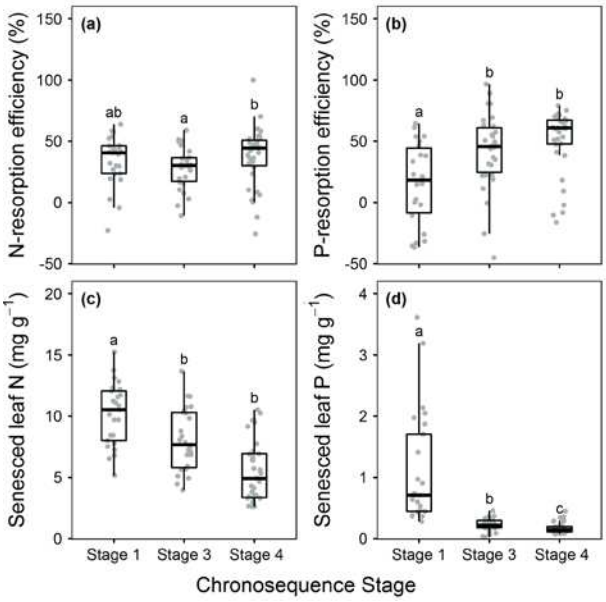

Figure 4. Nutrient resorption efficiency and proficiency for species in different soil development stages across the Jurien Bay chronosequence: (**a**) nitrogen- (N) resorption efficiency; (**b**) phosphorus- (P) resorption efficiency; (**c**) N-resorption proficiency and; (**d**) P-resorption proficiency. Box-plots with medians, 25th and 75th percentiles. Whiskers extend to 1.5 times the interquartile range. Data presented beyond whiskers represent outliers. Different letters indicate significant differences ($P<0.05$) among dune stages within each panel, based on Tukey`s HSD test.

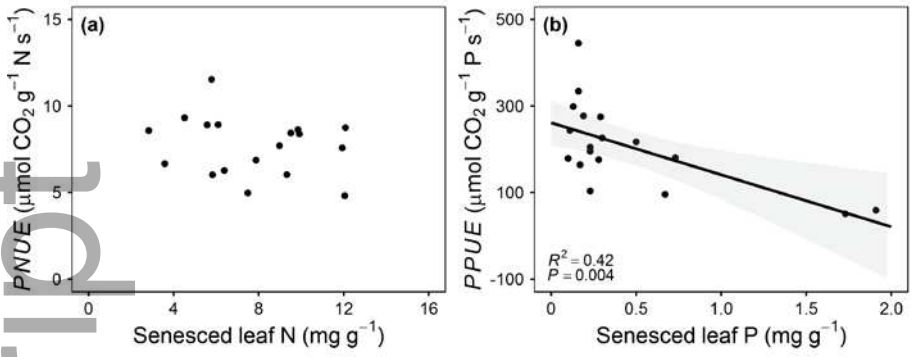

Figure 5. Correlation between nutrient-based rates of CO_2 assimilation and nutrient resorption proficiency for species within the Jurien Bay dune chronosequence: (**a**) correlation between nitrogen- (N) based rates of CO_2 assimilation (*PNUE*) and N resorption proficiency and; (**b**) correlations between phosphorus- (P) based rates of CO_2 assimilation (*PPUE*) and P resorption proficiency. Individual data points represent mean values for each species (n = 18), with regression lines, 95% confidence intervals (in grey) and R^2 values for the statistically significant relationships.

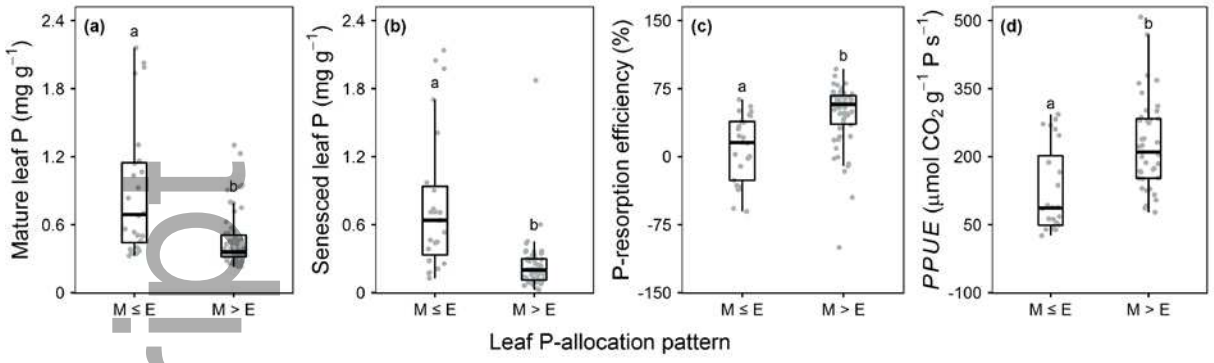

Figure 6. Leaf trait data for plants with contrasting phosphorus- (P) allocation patterns across the Jurien Bay chronosequence: (**a**) mature leaf P; (**b**) senesced leaf P; (**c**) P-resorption efficiency and; (**d**) photosynthetic P use efficiency (PPUE). Abbreviations: M ≤ E indicate species in which the cellular [P] of the epidermis was either higher or equivalent to that of the mesophyll; and M > E indicate species in which the cellular [P] was significantly higher in the mesophyll. Box-plots with medians, 25th and 75th percentiles. Whiskers extend to 1.5 times the interquartile range. Data presented beyond whiskers represent outliers. Different letters indicate significant differences (P<0.05) among dune stages within each panel, based on Tukey`s HSD test.

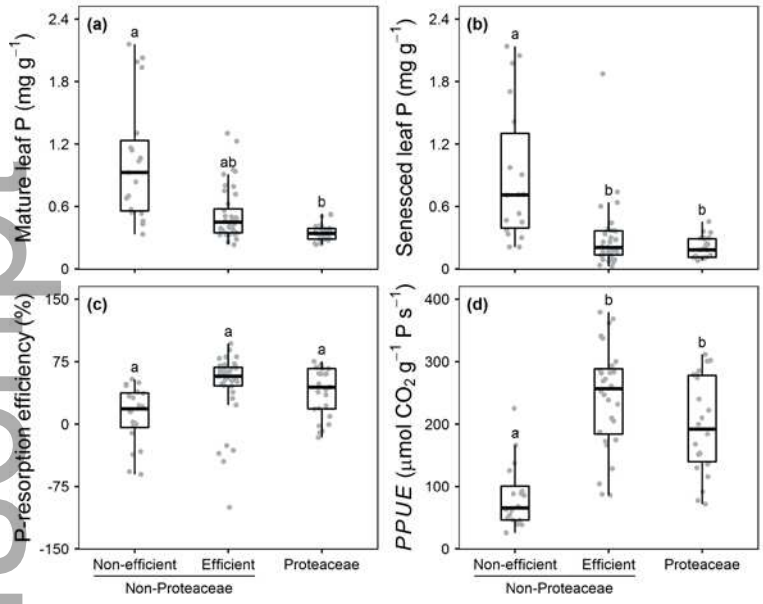

Figure 7. Leaf trait data for distinct plant groups across the Jurien Bay dune chronosequence: (**a**) mature leaf phosphorus (P); (**b**) senesced leaf P; (**c**) P-resorption efficiency and; (**d**) photosynthetic P use efficiency (PPUE). Non-proteaceae species were considered P-efficient whenever the mean PPUE ≥ 200 µmol CO_2 g^{-1} P s^{-1}. Box-plots with medians, 25th and 75th percentiles. The whiskers extend to 1.5 times the interquartile range. Data presented beyond whiskers represent outliers. Different letters indicate significant differences (P<0.05) among stages within each panel, based on Tukey`s HSD test.